UNIVERSITÀ DEL PIEMONTE ORIENTALE

School of Medicine

Department of Health Sciences

Master's Degree in Medical Biotechnologies

Integration of [^{18}F]FDG-PET radiomics with liquid biopsy improves outcome prediction in newly diagnosed diffuse large B-cell lymphoma

TUTOR:

Chiar.mo Prof. Gianluca GAIDANO

Firmato digitalmente da Gianluca Gaidano
Data: 18.02.2026 10:30:08 CET
Organizzazione: UNIVERSITA' DEGLI STUDI DEL PIEMONTE ORIENTALE/01943490027

Candidate: Mousa Jbara

Matricula number: 20058796

Academic Year 2024/2025

INDEX

ABSTRACT

Diffuse large B-cell lymphoma (DLBCL) is the most common and clinically heterogeneous subtype of non-Hodgkin lymphoma, with approximately one-third of patients experiencing relapse or refractory disease despite standard R-CHOP chemoimmunotherapy. Early identification of individuals at high risk of treatment failure remains a critical unmet clinical need. Traditional prognostic tools, including the International Prognostic Index (IPI) and cell-of-origin (COO), only partially capture the biological complexity that drives variable outcomes. Therefore, more refined, and integrative biomarkers are required to improve patient stratification at diagnosis.

This thesis investigates the combined prognostic potential of quantitative [^{18}F]FDG-PET radiomics and circulating tumor DNA (ctDNA) analysis in newly diagnosed DLBCL. Using a real-life cohort of 120 patients uniformly treated with R-CHOP, metabolic parameters were extracted from baseline PET/CT scans following a standardized SUV threshold of 4.0. These included total metabolic tumor volume (tMTV), total lesion glycolysis (tTLG), maximum standardized uptake value (SUVmax), and the maximum distance between lesions (Dmax). In parallel, plasma samples were analyzed using CAPP-seq to quantify baseline ctDNA levels and assign LymphGen molecular subtypes.

Baseline tMTV, tTLG, and Dmax demonstrated strong and independent prognostic value for progression-free survival (PFS) and overall survival (OS) even after adjusting for ctDNA levels. These PET parameters were combined into a unified variable, termed high-risk PET, which, together with ctDNA-high status, formed a two-factor prognostic model. This integrated model outperformed IPI, thereby markedly improving early risk prediction compared with clinical factors alone. Incorporation of LymphGen molecular clustering further refined prognostic accuracy. The three-factor model significantly improved outcome stratification and identified a very high-risk subgroup with extremely poor long-term outcomes.

These findings show that integrating PET radiomics with liquid biopsy provides a more accurate and biologically informed prediction of treatment failure, supporting the adoption of combined imaging-genomic strategies for personalized management and clinical trial stratification in DLBC.

1. INTRODUCTION

1.1. Diffuse large B-cell lymphoma

Diffuse large B-cell lymphoma (DLBCL) is the most common form of non-Hodgkin lymphoma (NHL). It is an aggressive disease, often marked by rapidly growing lymph nodes and systemic symptoms, requiring Immediate medical intervention (Pasqualucci et al., 2011) .

DLBCL is most commonly diagnosed in people in their mid-60s, with about 30% of cases occurring in those over 75. While most patients have no prior history of lymphoma, DLBCL can sometimes arise from an existing but undiagnosed low-grade B-cell lymphoma. Research suggests that the disease has a complex and multifactorial origin, influenced by genetic predisposition, immune system dysfunction, clinical factors, and external triggers such as viral infections, environmental exposures, and occupational hazards (Sehn & Salles, 2021).

The standard treatment is chemoimmunotherapy (CI) with R-CHOP regimen (rituximab, cyclophosphamide, doxorubicin, vincristine, and prednisone), which leads to cure in approximately over 60% of patients (Pasqualucci et al., 2011; Roschewski et al., 2014; Tilly et al., 2015) . More recently, the combination of polatuzumab vedotin with rituximab, cyclophosphamide, doxorubicin, and prednisone (Pola-R-CHP) has also emerged as a frontline standard, particularly in patients with intermediate- to high-risk DLBCL based on the international prognostic index (IPI) score (Tilly et al., 2022) .

However, the heterogeneity in the molecular landscape of DLBCL presents challenges in assessing response to treatment, prognosis, and identification of patients with early relapsing/refractory disease after first-line chemoimmunotherapy (Moia et al., 2025) .

1.2. Cell of origin

DLBCL occurs as a result of an expansion and progressive accumulation of mature and malignant B lymphocytes, at different stages of differentiation. During B lymphocyte ontogeny, after arising in the bone marrow (BM), these cells migrate to secondary lymphoid tissues, where they encounter their respective antigens that stimulate the development of secondary follicles. Within the germinal centers (GCs) of these follicles, B lymphocytes are involved in clonal expansion somatic hypermutation, and antibody affinity maturation processes that are essential for the production of high-affinity antibodies (De Silva & Klein, 2015; Mesin et al., 2016) .

DLBCL results from the malignant transformation of mature B-cells that have experienced the GC reaction. GCs are dynamic compartments that form when B-cells are challenged by a foreign antigen and represent the primary site for clonal expansion and antibody affinity maturation (De Silva & Klein, 2015; Mesin et al., 2016) . Dysregulation of these processes can disrupt normal B-cell maturation and promote lymphomagenesis.

Using Gene expression profiling (GEP) DLBCL can be classified based on its cell of origin (COO) into three main subtypes: *i)* germinal center B-cell (GCB)-like subtype shares gene expression patterns with normal GC B-cells and derives from GC light zone, *ii)* activated B-cell (ABC)-like subtype resembles normal activated B-cells and originates from a later stage of GC B-cells differentiation,. The remaining cases fall into an unclassifiable category, lacking clear characteristics of either group (Alizadeh et al., 2000; Basso & Dalla-Favera, 2015; Chapuy et al., 2018)(Figure 1).

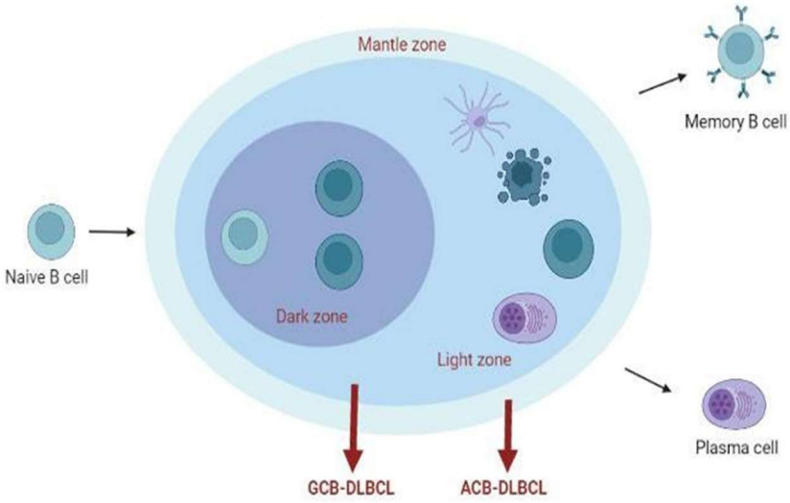

Figure 1. Cell of origin of DLBCL subtypes

The genetic of GCB-DLBCL is thought to originate from light-zone GC B-cells, displays high level expression of the master regulator B-cell lymphoma/leukemia 6 (*BCL6*) and harbors hypermutated immunoglobulin (Ig) genes with ongoing somatic hypermutation (SHM); While ABC-DLBCL arises from B-cells that have passed through the GC and are on the path to becoming plasma cells, shows activation of nuclear factor kappa-light-chain- enhancer of activated B-cells (NF-κB) and B-cell receptor (BCR) signaling pathways, and upregulation of genes required for

plasmatic differentiation. DLBCL risk stratification, according to COO, has prognostic value upon R-CHOP treatment. ABC-DLBCL is generally associated with poorer responses to standard treatments compared to GCB-DLBCL ((Dunleavy & Wilson, 2014; Scott et al., 2015; Thieblemont et al., 2011)(Figure 2).

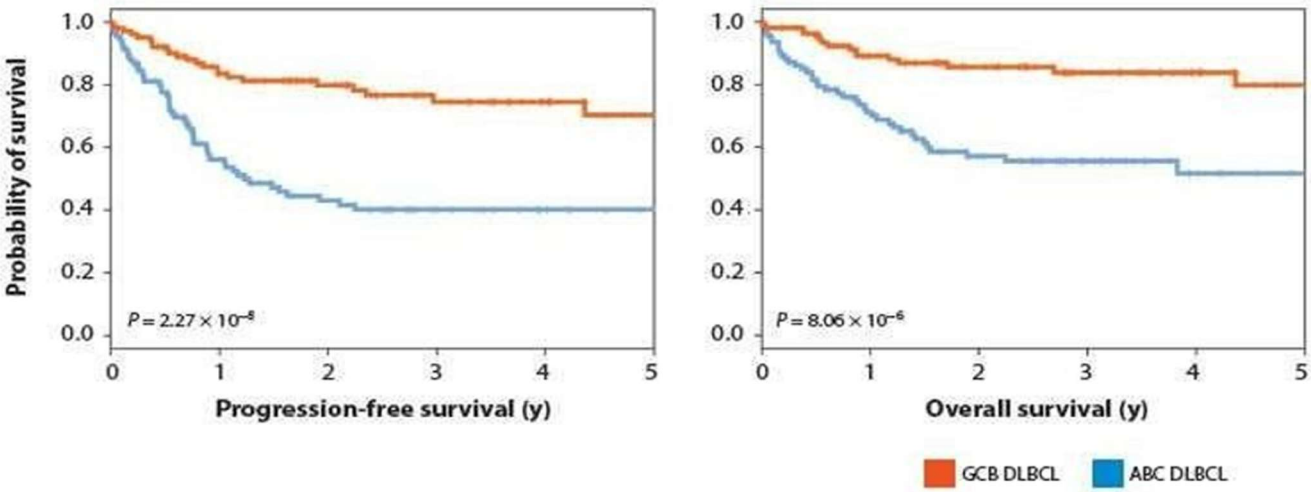

Figure 2. Outcome of GCB-DLBCL and ABC-DLBCL with R-CHOP

1.3. Molecular pathogenesis of DLBCL

The pathogenesis of DLBCL involves numerous genetic alterations. Some of these are shared between the two main molecular subtypes GCB-DLBCL and ABC-DLBCL, while others are subtype-specific. Common genetic abnormalities found in both GCB- and ABC-DLBCL include: *i)* alterations in histone/chromatin-modifying enzymes; *ii)* dysregulation of BCL6 activity; *iii)* mechanisms enabling immune evasion; and *iv)* additional mutations, including somatic copy number alterations (SCNAs) and structural variants (SVs).

i) Alterations in histone/chromatin modifiers

One of the most frequent genetic events in DLBCL is somatic mutation of of lysine-specific methyltransferase 2D (*KMT2D*) gene, found in approximately 30% of cases (Morin et al., 2011; Pasqualucci et al., 2011).*KMT2D* encodes a member of the SET1 family of histone methyltransferases, which promotes an active chromatin state by trimethylating histone H3 at

lysine 4 (H3K4) (Shilatifard, 2012) .These mutations are predominantly truncating or missense events that disrupt enzymatic activity by deleting the C-terminal domains, including the critical SET domain (Morin et al., 2011; Pasqualucci et al., 2011) .

Additionally, over one third of DLBCL patients shows somatic mutations and/or deletions affecting the acetyltransferase gene coding for CREB binding protein (*CREBBP*) (∼50% in GCB-DLBC and ∼30% in ABC-DLBCL) (Pasqualucci et al., 2011).DLBCL- associated mutations and small insertion or deletion (indels) disrupt the function of the CREBBP/EP300 proteins either by removing the histone acetyltransferase domain or by introducing amino acid changes within this domain, which cause decreased affinity for Acetyl-coenzyme A (CoA) (Pasqualucci et al., 2011).

ii) Dysregulation of BCL6 activity

Mutations affecting *BCL6* are present in 61% of DLBCL cases, with a higher prevalence in GCB-DLBCL (>70%) compared to ABC-DLBCL (~44%). The main mechanisms of BCL6 deregulation are chromosomal translocations and SHM. Translocations replace the *BCL6* promoter with heterologous promoter elements from translocation partners, while SHM affects the first intron and, less frequently, the first non-coding exon. Additionally, BCL6 function may be indirectly influenced by mutations that impair its regulation, such as those affecting CREBBP/EP300, which are required for the acetylation-mediated inactivation of BCL6 (Bereshchenko et al., 2002; Pasqualucci et al., 2011; Pasqualucci & Dalla-Favera, 2018a) . However, the accumulation of *BCL6* mutations has not been shown to have any association with disease progression (Iqbal et al., 2007).

iii) Immune evasion

Due to different genetic and epigenetic mechanisms, DLBCL commonly fails to express cell surface molecules, such as major histocompatibility complex (MHC) class I, which is required for the recognition of tumor cells by immune effector cells. These mechanisms include inactivating mutations and deletions within the β2-microglobulin (*BM2*) locus, thus preventing the coding of BM2 protein, necessary for the formation of cell surface expression of the human leukocyte antigen class I (HLA-I), involved in the CD8+ cytotoxic T cells recognition (Challa-Malladi et al., 2011) .

iv) Additional lesions

Several other genetic lesions contribute to DLBCL pathogenesis. Studies have shown that *TP53* mutations are present in about 20% of DLBCL cases as an independent predictor of poorer prognosis. *TP53* mutations usually result in loss-of-function and can occur in the DNA binding domain, with a negative prognostic impact. (Karube et al., 2018; Kerbauy et al., 2004; Xu-Monette et al., 2012, p. 20012; Young et al., 2007) .Forkhead box protein O1 (*FOXO1*) gene mutations were detected in 8.6% of DLBCL cases. These mutations, localized in the first exon, in particular in the N-terminal region and in the DNA binding domain, comprise amino acid changes, likely preventing the inactivation of FOXO1 in response to phosphoinositide 3-kinase (PI3K) signaling (Karube et al., 2018; Trinh et al., 2013) .This transcription factor is a key player during B-cell differentiation, and its activity is negatively regulated by PI3K/AKT pathway (Dominguez-Sola et al., 2015) . As consequence, alterations within *FOXO1* decrease overall survival (OS) in patients treated with R-CHOP (Trinh et al., 2013) .

1.4. Genetic lesions associated with GCB-DLBCL

In DLBCL, certain genetic abnormalities are more common with GCB-DLBCL. These include: *i)* chromosomal translocations involving the B-cell lymphoma/leukemia 2 (*BCL2*) and myelocytomatosis viral oncogene homolog (*MYC*) genes; *ii)* mutations of the enhancer of zeste homolog 2 (*EZH2*) methyltransferase gene; *iii)* mutations of the tumor necrosis factor- receptor superfamily member 14 (*TNFRSF14*) and iv) alterations affecting B-cell migration.

i) Chromosomal translocations of BCL2 and MYC:

BCL2 is a key antiapoptotic protein that prevents cell death and is found in most tissues. However, it is normally absent in GC because GC B-cells need to maintain a default proapoptotic program. In about 30% of GCB-DLBCL cases, the t(14;18) translocation juxtaposes the *BCL2* coding exons under the control of the immunoglobulin (IG) locus, resulting in its constitutive expression. Deregulation of BCL2 has been associated with an inferior outcome, particularly coupled with MYC deregulation (S. L. Barrans et al., 2003).

The *MYC* gene encodes for a transcription factor that regulates many critical cell functions, including cell growth, energy use, differentiation, and programmed cell death. MYC is ectopically and constitutively expressed in 10% to 14% of GCB- DLBCLs, often as the result of chromosomal translocations that join its intact coding domain to the IG heavy or light chains loci (Karube &

Campo, 2015). The presence of *MYC* translocations has been linked to worse prognosis in DLBCL (S. Barrans et al., 2010). *MYC* and *BCL2* chromosomal translocations coexist in 5% to 10% of DLBCL patients (Burotto et al., 2016) .

In the 2016 World Health Organization (WHO) Classification, a new entity termed high-grade B-cell lymphoma (HGBL) was introduced, defined by the presence of *MYC* and *BCL2* and/or *BCL6* rearrangements, DLBCL morphology, and a poor prognosis when treated with R-CHOP chemotherapy (Quintanilla-Martinez, 2017) .In the most recent WHO Classification, this category has been refined to incorporate advances in molecular characterization. The entity HGBL with MYC and *BCL2* and/or *BCL6* rearrangements is now restricted to cases harboring concurrent MYC and *BCL2* rearrangements (with or without *BCL6*) and is designated as DLBCL/HGBL-MYC/BCL2. Cases with MYC and BCL6 rearrangements alone have been reclassified as either DLBCL, not otherwise specified (DLBCL-NOS) or HGBL, NOS (WHO-HAEM5, 2022). These double hit (DH) lymphomas typically display high-grade morphology and an aggressive clinical course, with poor response to standard R-CHOP chemoimmunotherapy (S. Barrans et al., 2010) .

Mutations of EZH2 methyltransferase:

EZH2 encodes a SET-domain histone methyltransferase that is responsible for trimethylating the lysine 27 residue of histone H3 (H3K27me3)(Czermin et al., 2002) .Approximately 22% of GCB-DLBCL display heterozygous *EZH2* gene mutations, which in most cases replace a single evolutionarily conserved residue (Y641) within the protein SET domain, enhancing its ability to catalyze the addition of H3K27me3 mark (Morin et al., 2011; Sneeringer et al., 2010) .

ii) Mutations in TNFRSF14:

TNFRSF14 encodes for a member of the tumor necrosis factor-receptor superfamily that is expressed in both T and B-cells and can deliver opposing signals based on its specificity for diverse ligands(Steinberg et al., 2011) .High *TNFRSF14* expression correlates with poor OS and progression-free survival (PFS)(Carreras et al., 2019). Deletions and mutations of *TNFRSF14*, including missense (~50%), nonsense (~40%), and frameshift (2.5%) events confined to the exons encoding for its ectodomain, are recurrently found in DLBCL and segregate with the GCB subtype (30% of cases)(Boice et al., 2016) One mechanism underlying the tumorigenic effect of

TNFRSF14 loss is the inhibition of cell-cell interactions between this receptor and its ligand B- and T-lymphocyte attenuator (BTLA), which induces a tumor-supportive microenvironment (Boice et al., 2016).

iii) Alterations in B-Cell Migration:

The GC, specialized microstructure in the secondary lymphoid tissues, physiologically produces plasma cells (PCs) secreting antibodies and memory B-cells upon infection or immunization.(Stebegg et al., 2018). The confinement of B-cells within this microenvironment is modulated by the activity of two GC-specific-G-protein– coupled receptors (GPCRs): sphingosine-1-phosphate receptor 2 (S1PR2) and the orphan purinergic receptor P2RY8 (Green et al., 2012) .In response to lipid ligands, these receptors recruit two closely related G proteins (Ga12 and Ga13) and stimulate RHOA activity through specific guanine nucleotide exchange factors, to ultimately suppress pAKT signaling and cell migration. GCB-DLBCL, but not ABC-DLBCL, displays recurrent inactivating mutations in several components of this pathway, including the *S1PR2*, *GNA13*, and, more rarely, *ARHGEF1* and *P2RY8* genes (overall, ;30% of cases) (Cattoretti et al., 2009; Muppidi et al., 2014).Accordingly, deletion of these genes in the mouse is associated with disruption of the GC architecture, followed by dissemination of GC B-cells to the peripheral blood and bone marrow, eventually leading to the development of lymphomas that exhibit features of GCB-DLBCL (Cattoretti et al., 2009; Muppidi et al., 2014).

1.5. Genetic lesions associated with ABC-DLBCL

The key biology of ABC-DLBCL is defined by alterations that result in the constant activation of the NF-κB pathway, which is essential for the survival of ABC-DLBCL cells(Pasqualucci et al., 2011). These alterations include: *i)* mutations in the BCR signaling pathway; *ii)* mutations of myeloid differentiation primary response 88 (*MYD88*); *iii)* mutations of tumor necrosis factor alpha-induced protein 3 (*TNFAIP3*); and *iv)* lesions blocking terminal B-cell differentiation.

i) ***Mutations in the BCR signaling pathway***

ABC-DLBCL exhibits a "chronic active" form of BCR signaling, driven by genetic changes that affect key components of the pathway (Davis et al., 2010). In 21% of cases, this is

due to gain-of-function mutations in the immunoreceptor tyrosine-based activation motifs of cluster of differentiation 79B (CD79B), which sustain BCR signaling by disrupting negative feedback mechanisms (Davis et al., 2010). In 9% of cases, mutations affect the gene encoding the caspase recruitment domain family member 11 (CARD11)(Lenz et al., 2008), a critical part of the "signalosome" complex necessary for proper BCR signal transduction (Thome, 2004). These mutations primarily affect the exons encoding the protein's coiled-coil domain, enhancing CARD11's ability to activate NF-κB target genes (Davis et al., 2010; Knies et al., 2015).

ii) ***Mutations of MYD88***

Around 30% of ABC-DLBCL cases involve mutations that cause a hotspot L265P substitution in the hydrophobic core of the MYD88 Toll/interleukin-1 receptor (TIR)-domain. This adaptor molecule is essential for transmitting signals from the Toll-Like Receptor (TLR) to the NF-κB transcription complex .(Lam et al., 2008, p. 200; Ngo et al., 2011, p. 201) In particular, the L265P substitution triggers the activation and phosphorylation of interleukin-1 receptor-associated kinase 4 (IRAK4) by promoting the spontaneous formation of a protein complex containing both IRAK1 and IRAK4. This complex, in turn, activates NF-κB and initiates the Janus kinase/signal transducers and activators of transcription (JAK/STAT3) pathways (Rhyasen & Starczynowski, 2015).

iii) Aberrations of TNFAIP3

Approximately 30% of ABC-DLBCL cases show biallelic mutations and/or focal deletions that inactivate the tumor necrosis factor alpha–induced protein 3 (*TNFAIP3*) gene, which encodes a dual-function ubiquitin-editing enzyme involved in negatively regulating NF-κB responses triggered by TLR and BCR signaling (Boone et al., 2004; Compagno et al., 2009; Kato et al., 2009).The loss of TNFAIP3/A20 function may contribute to lymphomagenesis by allowing NF-κB responses to persist inappropriately for extended periods (Compagno et al., 2009; Kato et al., 2009).

iv) Lesions blocking terminal B-cell differentiation

In ABC-DLBCL, the genetic-driven, constant activation of NF-κB is often accompanied by alterations that impede terminal B-cell differentiation (Pasqualucci & Dalla-Favera,

2018b).Notably, 25% of cases exhibit biallelic loss-of-function mutations or deletions in the PR domain-containing protein 1 (PRDM1)/β-interferon gene positive regulatory domain I-binding factor (BLIMP1), a transcriptional repressor critical for B-cell plasmacytic differentiation and essential for plasma cell (PC) development (Pasqualucci et al., 2006).

1.6. DLBCL subtypes and novel molecular clusters

GEP has been used to classify DLBCL into subgroups based on the COO, ABC, GCB, and unclassified, each of which is linked to different responses to chemotherapy and targeted therapies (Alizadeh et al., 2000; Rosenwald et al., 2002). This classification accounted for some of the heterogeneity in the clinical outcome following R-CHOP chemotherapy, but it does not fully account for the diverse responses and outcomes observed with R-CHOP or targeted treatments. The extreme genetic and phenotypic heterogeneity of DLBCL continues to pose challenges to the development of precision therapies (Wright et al., 2020).

To address this complexity, various mathematical-based clustering methods have been employed to stratify DLBCL tumors into genetic subtypes that are characterized by genomic aberrations in subtype specific hallmark genes. Integrating genomic data from multiple analytical platforms has enabled the identification of genes recurrently altered by mutations, translocations, and copy-number changes, providing the basis for a genetic classification of DLBCL (Chapuy et al., 2018; Schmitz et al., 2018) .The clinical relevance of these genetic subtypes was highlighted by their association with outcomes following R-CHOP therapy (Wright et al., 2020) .

In 2018, Chapuy and colleagues performed whole-exome sequencing (WES) with an expanded bait set to capture known structural varia SVs in 304 newly diagnosed DLBCL cases. They identified five distinct molecular clusters (C1–C5) with unique genetic signatures, along with an additional subset without detectable alterations (C0) (Chapuy et al., 2018) .

Cluster 5. Predominantly characterized by *BCL2* gain-of-function alterations, mutations in *MYD88*^{L265P}, and *CD79B* genes (Chapuy et al., 2018) .

Cluster 1. Mainly containing *BCL6* SVs and mutations in components of the NOTCH2 signaling pathway, along with multiple genetic bases of immune escape, including inactivating mutations. The majority of C1 and C5 DLBCLs were classified as ABC-type tumors by transcriptional profiling, suggesting different targeted treatment strategies: inhibition of BCR/TLR

signaling and BCL2 in C5, and targeting NOTCH, BCL6, and immune evasion in C1(Chapuy et al., 2018) .

Cluster 3. Marked by *BCL2* alterations, frequent mutations in chromatin modifiers (*KMT2D, CREBBP, EZH2*) and *PTEN* inactivation (Chapuy et al., 2018) .

Cluster 4. Identified by mutations in immune evasion molecules (*CD83*), BCR/PI3K intermediates (*SGK1*), NF-κB modifiers (*CARD11*), and RAS/JAK/STAT pathway members. C4 and C3 represent distinct GCB tumor subsets, with potential therapies targeting BCL2, PI3K, and epigenetic modifiers in C3 GCB tumors, and JAK/STAT and BRAF/MEK1 blockade in C4 GCB-DLBCLs (Chapuy et al., 2018) .

Cluster 2. Characterized by frequent biallelic inactivation of *TP53* through mutations and 17p copy loss, with both GCB and ABC subtypes represented (Chapuy et al., 2018)

Cluster 0. A small subset of DLBCLs, defined as cluster 0 (C0) lacked defining genetic drivers (Chapuy et al., 2018).

In this study, the prognostic analysis revealed that patients with C0, C1, and C4 subtypes had more favorable outcomes, whereas those with C3 and C5 clusters exhibited poorer prognosis (Chapuy et al., 2018)

In the same year, Schmitz and his group analyzed approximately 500 DLBCL cases using exome and transcriptome sequencing, array-based DNA CN analysis, and targeted resequencing 372 genes to identify more recurrently altered genes and pathways (Schmitz et al., 2018). They identified four genetic DLBCL subtypes, applying the predictor algorithm Genclass: MCD (based on the co-occurrence of *MYD88*^{L265P} and *CD79B* mutations), BN2 (based on *BCL6* fusions and *NOTCH2* mutations), N1 (based on *NOTCH1* mutations), and EZB (based on *EZH2* mutations and *BCL2* translocations). These subtypes differed in gene expression signatures and responses to immunochemotherapy, with favorable survival observed in BN2 and EZB subtypes, while MCD and N1 subtypes had worse outcomes (Schmitz et al., 2018) .

Building on these findings, Wright *et al,* combined the genetic profiles from these two studies to develop the LymphGen algorithm that provides a probabilistic classification tool for DLBCL tumor from an individual patient into a genetic subtype (Wright et al., 2020) . They define a genetic subtype as a group of tumors that is enriched for genetic aberrations in a set of subtype predictor genes. These subtype predictor genes are identified by considering each possible

combination of genetic aberrations. LymphGen uses the presence or absence of each subtype predictor feature to provide a probability that a tumor belongs to the subtype(Wright et al., 2020).

To display the genetic composition of the subtypes, they selected a set of genetic features that were significantly associated with a subtype ($p \leq 0.01$) and were present in >10% of the subtype. First, they chose seeds representing the four previously identified genetic subtypes: MCD (including *MYD88*^{L265P} and *CD79B* mutations), BN2 (including *BCL6* translocations and *NOTCH2* mutations), N1 (including *NOTCH1* mutations), and EZB (including *EZH2* mutations and *BCL2* translocations). They therefore formed a seed class of cases with *TP53* features, termed ‘‘A53". In addition, they created a second new seed class based on the features of *SGK1* and *TET2* genes, which is termed ‘‘ST2".

This classification breaks DLBCLs into seven genetic subtypes that differ in oncogenic pathway activation, gene expression phenotype, tumor microenvironment, survival, and potential therapeutic targets (Wright et al., 2020) .

Recent advances in the molecular characterization of diffuse large B-cell lymphoma (DLBCL) have led to the development of DLBclass, a next-generation probabilistic classifier designed to prospectively identify the five genetically defined clusters (C1–C5). DLBclass integrates mutations, SCNAs, and SVs, while demonstrating that additional parameters such as tumor ploidy or COO status, reflecting the natural enrichment of ABC tumors in C1 and C5 and GCB tumors in C3 and C4, while C2 remains COO-independent. Importantly, the model also clarified additional cluster-specific alterations, including new mechanisms of NOTCH2/NF-κB activation in C1, enrichment of MYC/BCL2 double translocations in C3, and C4 features overlapping with T-cell/histiocyte-rich LBCL . (Chapuy et al., 2025a)

Compared with LymphGen, DLBclass captures a larger fraction of DLBCL cases and provides more actionable genetic information, offering a practical and comprehensive framework for personalized treatment approaches .(Chapuy et al., 2025b) .

1.7. DLBCL diagnosis, prognostic factors and treatment

DLBCL istypically diagnosed through an excisional biopsy of a suspicious lymph node (LN), which reveals large clusters of cells that disrupt the structural integrity of the follicle center and test positive for pan B-cell markers like CD20 and CD79A. The COO is determined using immunohistochemical (IHC) stains or GEP (Liu & Barta, 2019) .

The standard treatment for DLBCL patients is R-CHOP chemoimmunotherapy, which includes rituximab, an antibody targeting the CD20 protein found on the surface of B-cells along with chemotherapy drugs cyclophosphamide, doxorubicin, vincristine, and prednisone (Chiappella et al., 2013; Kwak, 2012) .With this regimen, approximately 60-70% of patients with DLBCL are cured of disease. However, 30-40% of patients will relapse or, in a small patient's subset, be refractory to R-CHOP therapy (Liu & Barta, 2019).Failure of R-CHOP therapy is mainly due to primary refractoriness or relapses following an initial complete response (CR) (Coiffier & Sarkozy, 2016) .

A more recent advancement in frontline therapy for DLBCL is the use of polatuzumab vedotin in combination with rituximab, cyclophosphamide, doxorubicin, and prednisone (Pola-R-CHP). This regimen has emerged as a new standard of care, particularly for patients with intermediate- to high-risk disease according to the IPI score ((Tilly et al., 2022) .

Moreover, the different genetic subtypes of DLBCL can influence treatment decisions. For example, lesions affecting the BCR-dependent NF-κB pathway are common in the BN2, MCD, and A53 subtypes, suggesting these may be responsive to Bruton tyrosine kinase inhibitors (BTKis). Specifically, MCD-like tumors, which harbor *MYD88*^{L265P} and *CD79B* mutations, have shown a high response rate (≥80%) to ibrutinib in relapsed cases (Grommes et al., 2017; Lionakis et al., 2017; Wilson et al., 2015) . Additionally, the MCD model, driven by autocrine IL-10 receptor signaling activating JAK1 and STAT3 , has shown responsiveness to the selective JAK1 inhibitor INCB040093 when combined with a PI3Kδ inhibitor in non-GCB DLBCL(Phillips et al., 2018) .EZB subtype, which carries an *EZH2* mutation, may be more responsive to EZH2 inhibitors (Wright et al., 2020). Furthermore, *BCL2* alterations observed in MCD, BN2, and EZB models suggest that therapies like venetoclax or navitoclax could be beneficial for these genetic subtypes (Mathews Griner et al., 2014) .

GEP has provided valuable insights into DLBCL biology and led to the adoption of IHC algorithms in routine clinical practice. The identification of DH lymphomas, detected by fluorescence in situ hybridization (FISH) and characterized by translocations involving *MYC* and either *BCL2* or *BCL6*, is critical due to the poor prognosis associated with R-CHOP. DH or triple hit (TH) lymphomas, which involve rearrangements of *MYC* with *BCL2* and *BCL6*, are associated with a highly aggressive clinical course, poor response to conventional therapies, and high relapse rates (Green et al., 2012; Rosenthal & Younes, 2017) .

1.8. PET parameters role in DLBCL

Positron emission tomography with [^{18}F]fluorodeoxyglucose ([^{18}F]FDG-PET/CT) has emerged as an essential imaging modality in the assessment and management of DLBCL (Ceriani et al., 2025). Baseline PET/CT not only improves disease staging by detecting otherwise occult nodal and extranodal disease but also provides quantitative biomarkers that reflect whole body tumor burden and biology. These parameters are critical for clinicians to determine appropriate treatment strategies and make prognostic predictions .(Cottereau et al., 2020; Frood et al., 2021)

Among these parameters, total metabolic tumor volume (MTV) and total lesion glycolysis (TLG) have been widely recognized for their prognostic value across multiple cohorts. MTV quantifies the total volume of all FDG-avid lesions throughout the body, thereby representing the entire metabolically active tumor burden. TLG, on the other hand, provides a comprehensive measure of total metabolic activity across all tumor sites (Eertink et al., 2022) . Numerous studies have shown that higher MTV/TLG values at baseline are indicative of more extensive disease and worse prognosis, suggesting that patients with high MTV may benefit from more aggressive or alternative therapeutic strategies, such as immunotherapy or targeted treatments (Sasanelli et al., 2014; Vercellino et al., 2020). Therefore, they play a pivotal role in identifying high-risk patients early, thus enabling personalized treatment approaches (Eertink et al., 2022).

Beyond MTV and TLG, the peak standardized uptake value (SUV peak) is another significant PET parameter that has been used to predict patient outcomes. SUV peak measures the intensity of FDG uptake within the most metabolically active tumor area, providing additional information on the aggressiveness of the lymphoma . SUV peak has been shown to correlate with clinical outcomes and can be a valuable tool in distinguishing between patients who will respond to standard treatments and those who may require more intensive therapy (Zhang et al., 2019) .

Another important parameter is the maximum distance between lesions (Dmaxbulk), which quantifies the spatial distribution of the lymphoma within the body. This metric reflects the tumor's heterogeneity and the potential for dissemination. Studies have suggested that patients with larger distances between lesions may have a higher risk of progression or relapse, further emphasizing the need for individualized treatment planning (Cottereau et al., 2020) .

The integration of these PET-based radiomics features MTV, SUV peak, and Dmaxbulk into clinical models has greatly improved the ability to predict treatment outcomes in DLBCL patients. One such model, developed using data from the HOVON-84 trial, incorporated these PET

parameters alongside clinical factors such as age and performance status (Lugtenburg et al., 2020) . This integrated PET model has outperformed the traditional IPI, which has been the gold standard for risk stratification in DLBCL for over three decades. The clinical PET model demonstrated a significantly higher area under the curve (AUC) compared to IPI, indicating its superior predictive power. Specifically, the clinical PET model allowed for more accurate identification of high-risk patients who would benefit from tailored therapies, with a higher positive predictive value (PPV) and improved specificity and sensitivity (Mikhaeel et al., 2022) .

While the clinical PET model has shown superior performance, the ability to apply these radiomic features in clinical practice depends on the standardization of PET imaging and analysis methods (Barrington & Meignan, 2019; Eertink et al., 2022). Initiatives such as the imaging biomarker standardization initiative (IBSI) and the development of software tools like ACCURATE are aimed at making PET radiomics more reproducible and accessible across different clinical settings . Standardization efforts will facilitate the broader use of PET-based radiomics for personalized medicine in DLBCL, ensuring that patients receive the most effective treatment tailored to their individual disease characteristics .(Zwanenburg et al., 2020).

1.9. Liquid biopsy applications in DLBCL

Traditional diagnostic methods, such as tissue biopsy, often fail to fully capture the complexity of tumor heterogeneity across different anatomical compartments since it typically samples a single tumor site (Rossi et al., 2017). Moreover, tissue biopsy is an invasive procedure that presents challenges for obtaining serial samples, which are necessary for real-time disease monitoring and therapeutic assessment(Talotta et al., 2023)These limitations underscore the need to explore new approaches for personalizing treatment and improving patient outcomes (Rossi et al., 2017).

In recent years, liquid biopsy has emerged as a possible complementary tool integrating tissue biopsy for lymphoma molecular diagnostics and management. This minimally invasive approach enables the identification of disease-related biomarkers through accessible procedures such as blood drawing or the collection of body fluids like saliva, urine, cerebrospinal fluid (CSF), and stool. Liquid biopsy offers several advantages over conventional tissue biopsy, including the ability to capture tumor heterogeneity at multiple sites, support real-time disease monitoring, and

allow for longitudinal sampling across treatment (Heitzer et al., 2019; Liu & Barta, 2019; Moia et al., 2021) .

Liquid biopsy includes several tumor-derived components circulating in body fluids that provide important information about tumor biology, such as circulating tumor DNA (ctDNA), circulating tumor cells (CTCs), and extracellular vesicles (EVs) (Jamal et al., 2024; Savino et al., 2022) .

ctDNA refers to fragments of DNA shed by tumor cells into the blood. It reflects the genetic mutations present in the tumor and provides a dynamic view of disease status.

ctDNA is an emerging biomarker across oncology, including lymphomas and it could serve as both a prognostic factor and a quantitative proxy for disease burden (Kurtz et al., 2015, 2018) .

The limitations in accessing fresh tumor material from DLBCL tissue biopsies has prevented the rapid translation of DLBCL gene mutations into prognostic or predictive tools for clinical practice (Rossi et al., 2017).Therefore, alternative accessible sources of tumor DNA may help to complement the molecular diagnostic analyses that are routinely carried out on formalin-fixed paraffine-embedded (FFPE) tissue biopsies (Rossi et al., 2017).

In DLBCL, the use of ctDNA is a powerful tool for the detection of genetic alterations that otherwise might be missed in the tissue biopsy. Advanced sequencing technologies, such as cancer personalized profiling by deep sequencing (CAPP-seq), have demonstrated that ctDNA can detect hallmark genetic alterations associated with DLBCL subtypes, including mutations of *MYD88*, *CD79B*, and *EZH2*, making it a useful tool for disease genotyping, enabling molecular classification of DLBCL and guiding targeted therapies. Studies have shown a high concordance between ctDNA genotyping and tissue biopsy for detecting genetic alterations in DLBCL (Rossi et al., 2017; Scherer et al., 2016; Spina et al., 2018).

The molecular classification of DLBCL was established mainly on the tissue biopsy, enabling the identification of clinically relevant genetic subtypes with distinct features (Chapuy et al., 2018; Wright et al., 2020) . Recent evidence shows that LymphGen can also be applied reliably and effectively on ctDNA. Moia et al. has reported a 95.8% concordance rate in molecular cluster assignment between ctDNA and tissue biopsy, highlighting the reproducibility of molecular clustering on plasma (Moia et al., 2025).As with tissue biopsy studies, patients assigned to the A53 and MCD clusters exhibited poorer outcomes, while those in the ST2 and BN2 clusters showed significantly better outcomes (Moia et al., 2025).

In DLBCL, ctDNA has been quantified or used to track the tumor clonotypic immunoglobulin gene rearrangement for minimal residual disease monitoring (Kurtz et al., 2015; Roschewski et al., 2014) .

Pretreatment ctDNA levels have been identified as a key prognostic biomarker in DLBCL. Several studies have linked higher baseline ctDNA levels to poorer PFS and OS (Alig et al., 2021; Meriranta et al., 2022) . Moreover, baseline ctDNA levels could also be integrated with molecular clusters identified on the liquid biopsy, this combined approach of integrating multiple ctDNA-derived biomarkers enhances the prognostic accuracy and allows for more precise risk stratification of DLBCL patients (Moia et al., 2025).

In addition to pretreatment prognostic value, the dynamic changes in ctDNA levels during therapy have been shown to reflect treatment response in DLBCL (Lauer et al., 2022)These molecular response biomarkers offer an additional tool for monitoring treatment response and may integrate traditional methods such as PET/CT scans .(Roschewski et al., 2023)

Despite its potential, there are challenges to the widespread clinical adoption of liquid biopsy in DLBCL. These include the need for standardization in sample collection, processing, and analysis, as well as technical limitations in detecting low frequency mutations and tumor chromosomal translocations. These notions suggest that liquid biopsy is not a substitute for the tumor biopsy but instead provides complementary information in DLBCL (Rossi et al., 2017). Nevertheless, with ongoing technological progress, ctDNA analysis may be expected to become a part of routine clinical practice in DLBCL, enhancing personalized treatment and improving patient outcomes (Almasri et al., 2025) .

2. AIM OF STUDY

The aims of the present study are:

i) To assess the prognostic significance of ctDNA levels and LymphGen molecular clustering on ctDNA in newly diagnosed DLBCL patients;

ii) To evaluate the prognostic value of baseline PET/CT radiomics parameters;

iii) to integrate the prognostic value of ctDNA levels, molecular clusters, and PET/CT variables to improve outcome prediction in DLBCL.

3. MATERIALS AND METHODS

3.1. Patients

A real-life cohort of 120 newly diagnosed DLBCL patients consecutively referring to our institution were included in the study. Patients had a diagnosis of DLBCL not otherwise specified (NOS) and were treated with R-CHOP-based therapy. All cases were provided at baseline with: *i)* [^{18}F]FDG-PET/CT scans; *ii)* ctDNA from plasma; and *iii)* germline gDNA extracted from granulocytes for comparative purposes. Patients provided informed consent in accordance with Institutional Review Board requirements and the Declaration of Helsinki. The study was approved by the Ethical Committee of the Ospedale Maggiore della Carità di Novara associated with the Università del Piemonte Orientale (study number CE 120/19).

3.2. [^{18}F]FDG-PET/CT analysis

All PET/CT scans were acquired using the same protocol, following the procedural guidelines described by the European Nuclear Medicine Association (EANM). Specifically, each patient fasted for at least 6 hours before the examination and was injected with 2.5–3 Mbq/kg of [^{18}F]FDG with a blood glucose level below 200 mg/dL. After 60 ± 10 minutes, total-body images from the nasion to the proximal third of the femurs were acquired. Non-contrast low-dose CT co-registration images were gathered to perform the attenuation correction processing, and then the images were reconstructed on the three spatial axes: axial, sagittal, and coronal. Subsequently, using the free software LIFEx v 7.4.0, a semiautomatic segmentation was conducted on all evident lesions in each PET/CT scan using specific automatic segmentation tools available in the software and, when necessary, performing the manual exclusion of activity related to the presence of radioactive urine in the renal excretory or physiological uptake in the cardiac area with the aid of co-registration CT images. Data were then collected by two independent nuclear radiologists (any possible conflict was resolved by consensus) using the SUVmax ≥4.0 threshold, since the current literature suggests that a SUVmax ≥4.0 may represent a more robust, reliable, and reproducible threshold when compared to a SUVmax ≥41%. Finally, for each patient the SUVmax of the hottest lesion, the total (t) MTV, the tTLG and the distance between the two farthest hypermetabolic lesions (Dmax) were collected.

3.3. Separation of granulocytes from peripheral blood (PB)

Peripheral blood (PB) granulocytes were isolated using Ficoll gradient density centrifugation to obtain normal germline genomic DNA (gDNA). The PB was diluted at a 1:2 ratio with physiological saline (0.9% NaCl) and centrifuged at 1800 rpm for 25 minutes using Sigma Diagnostic™ Histopaque®-1077 Cell Separation Medium (Sigma-Aldrich, St. Louis, MO, USA) to separate granulocytes from mononuclear cells (monocytes and lymphocytes).

3.4. Extraction of normal gDNA

Normal gDNA was extracted using the "salting out" method (Miller et al., 1988). Cells were lysed with a Lysis Buffer containing Tris-HCl 1M (pH 8.2), NaCl 5M, and EDTA 0.5M, along with 20% sodium dodecyl sulfate (SDS), and then digested with 20 mg/ml proteinase enzyme (pronase E). The samples were incubated overnight at 37°C in a shaking incubator. Proteins were precipitated by adding 6M NaCl and removed after centrifugation at 3200 rpm for 20 minutes. DNA was then precipitated using pure ethanol, forming a milky, jelly-like substance which was collected with glass loops and washed three times in 75% ethanol. After evaporating the residual ethanol, the DNA was dissolved in TE Buffer (Tris-HCl 1M, pH 8.2, EDTA 0.5M).

3.5. Plasma ctDNA extraction

PB samples were collected in Cell-Free DNA BCT® tubes and centrifuged at 800 relative centrifugal force (RCF) for 10 minutes at 4°C to separate plasma from blood cells. The plasma was then centrifuged again at 13,000 rpm for 10 minutes at 4°C to remove any remaining cells. Plasma samples were stored at -80°C until DNA extraction. ctDNA was extracted from 2–3 ml plasma aliquots immediately after thawing, using the Maxwell® RSC LV ccfDNA Kit Custom (Promega Corporation, Madison, WI, USA). Quantification was performed with a Quantus Fluorometer using the QuantiFluor double-stranded DNA (dsDNA) System (Promega Corporation). The quality of the extracted ctDNA was evaluated with the 2100 Bioanalyzer Instrument (Agilent Technologies, Santa Clara, CA, USA).

3.6. DNA quantification and fragmentation

gDNA was quantified using the Quant-iT™ PicoGreen dsDNA Assay kit (ThermoFisher Scientific, Eugene, OR, USA). PicoGreen is a dye that selectively binds to double-stranded DNA, enabling an accurate measurement of DNA quantity. Fluorescence readings were taken with the Infinite F200 fluorometer (TECAN, Männedorf, Switzerland) using Magellan software. Measurements were made at an excitation wavelength of 485 nm and emission wavelength of 530 nm. A standard curve was generated by preparing serial 1:2 dilutions of DNA with known concentration. The Quant-iT™ PicoGreen assay was performed at a 1:200 dilution.

gDNA extracted from tissue samples were sheared by sonication using the M220 focused ultrasonicator (Covaris®, Woburn, MA, USA) before library preparation to produce DNA fragments of 250–300 base pairs. Fragment sizes were verified with the 2100 Bioanalyzer Instrument. In contrast, circulating tumor DNA (ctDNA) is naturally fragmented and was used directly for library construction without further fragmentation.

3.7. Library design for hybrid selection

A targeted resequencing gene panel was specifically designed for this project, covering the coding exons and splice sites of 109 genes (total target region: 199411 base pairs) that are frequently mutated in DLBCL and other B-cell malignancies.

3.8. CAPP-seq library preparation

The gene panel was analyzed in two sample types: *i)* plasma ctDNA collected at diagnosis; and *ii)* germline gDNA from matched granulocytes for comparison. NGS libraries were prepared using the KAPA HyperPrep Library Preparation Kit (KAPA Biosystems, Wilmington, MA, USA), with hybrid selection performed using the custom KAPA HyperChoice probes (Roche, Basel, Switzerland). Multiplexed libraries were sequenced using 300-bp paired end runs on MiSeq Illumina platform and 150-bp paired end runs on NextSeq550 Illumina platform. (San Diego, CA, USA).

3.9. Next generation sequencing

The sequencing workflow involves the following phases: *i)* generation of libraries containing the regions of interest; *ii)* sequencing; and *iii)* data analysis.

i) Generation of libraries

The library preparation using the KAPA HyperPrep Library Preparation Kit (KAPA Biosystems, Wilmington, MA, USA), begins with end repair and A-tailing reaction, which produces end repaired, 5'-phosphorylation, 3'-A-tailed dsDNA fragments, followed by the adapter ligation, during which dsDNA adapters with 3'-dTMP overhangs are ligated to 3'-dA-tailed molecules.

ii) Sequencing

Miseq and NextSeq550 Illumina sequencers are based on sequencing by synthesis technology, in which DNA libraries are transferred onto a solid support, called flowcell, to which they are linked by special adapters. On the flowcell the libraries are amplified by a method called bridge amplification, which generates clusters of identical DNA molecules, each derived from the amplification of a single molecule. Sequencing is based on the reversible cyclic termination method, with a by-synthesis approach, which includes three steps: the incorporation of the nucleotide, the detection of the fluorescence image and the cut.

In the first phase of the cycle, the DNA polymerase elongates a specific primer by adding a nucleotide covalently bound to a fluorophore. This presents a block on the 3'- OH of ribose which does not allow polymerization with other nucleotides. Each nucleotide base is bound to a fluorophore of a specific colour. It follows the detection step of the image that recognizes the specific emission wavelength of the fluorophore. Next, the cut removes both the fluorophore and the inhibitory group present at the 3'-OH end, allowing the beginning of a new cycle. Libraries were sequenced by pair-end sequencing using a 300-bp paired-end cycle kit. The library pool was denatured using 0.2N NaOH.

An amount of 9 to 12 pM denatured DNA was loaded into the MiSeq and 1.3 pM into the Nextseq550.

iii) Data analysis

During the sequencing run, the integrated software for real-time primary analysis (RTA, Real Time Analysis, Illumina) performs image analysis and identification of the bases and assigns a qualitative score (Phred score) to each base for each cycle. Once the primary analysis is completed, the MiSeq Reporter (Illumina, San Diego, CA, USA) software performs a secondary analysis on the data generated by the RTA through a series of procedures that include: i) de-

multiplexing, in which the data of different samples sequenced are pulled together based on the specific sample index sequences; ii) FASTQ generation, which are files containing all the reads obtained from sequencing.

FASTQ sequencing reads were deduped by using the FastUniq v1.1. Then, the deduped FASTQ sequencing reads were locally aligned to the hg19 version of the human genome using the BWA v.0.6.1 software with the default setting, and sorted, indexed, and assembled into a mpileup file, using SAMtools v.1. Somatic SNVs and small insertions and deletions (indels) were identified in tumor/normal paired samples using the somatic function of VarScan2. Multiple comparisons test was performed to compare the variant allele frequency (VAF) *versus* the mean allele frequency in unpaired normal gDNA samples to filter out variants below the base-pair resolution background frequencies across the target region. Only variants that had a significant call in Z-test were retained (Bonferroni adjusted $p \leq 6.11x10^{-8}$). Mutations were annotated using wANNOVAR (https://wannovar.wglab.org/). *TP53* variants that were scored as SNPs according to the International Agency for Research on Cancer TP53 database; https://tp53.isb-cgc.org/), intronic variants, mapping >2 bp before the start or after the end of coding exons, and synonymous variants were then filtered out. Splice-acceptor and splice-donor variants were annotated by using the SeattleSeq Annotation 138 tool (http://snp.gs.washington.edu/SeattleSeqAnnotation138). Among the remaining variants, only protein truncating variants (i.e., indels, stop codons and splice site mutations), as well as nonsynonymous variants, not included in the dbSNP 138 and reported as somatic in the COSMIC v96 database (https://cancer.sanger.ac.uk/cosmic), were retained. All the variants were visualized using IGV (Integrative Genomics Viewer) software (v2.8.0).

3.10. Copy-number variation analysis on ctDNA

Genome wide somatic copy number abnormalities (SCNA) was performed using the CNVkit software toolkit (version 0.9.10) in Python 3.11.4.Although CNVkit is not specifically designed for copy number alteration (CNA) analysis, as internal validation, the results of CNVkit were compared to ichorCNA, a tool intended for estimating the fraction of tumor in cell-free DNA from ultra-low-pass whole genome sequencing (WGS). CNVkit infers copy number variations (CNVs) from targeted capture sequencing data. Sequencing data (cfDNA BAM-files) from the CAPP-seq pipeline, including both on-target and off-target reads, were used as input. The target bin size was set to default. A reference file was built from 41 normal cfDNA samples; read depths

were median-centered and bias-corrected (GC-content, sequence repeats, target density) to produce normalized log2 read-depth values for each bin. To infer copy-number changes, "observed" normalized log2 read-depth values from patient samples were subtracted from the "expected" values in the reference file and bins were segmented using circular binary segmentation with the "droplow- coverage" option. We applied the GISTIC2.0 GenePattern module (version 6.15.30) to identify statistically significant CNVs. The thresholds used in our analysis were 0.3 for amplifications and 0.3 for deletions. GISTIC output files were processed and summarized using maftools R package (version 2.10.05).

3.11. Molecular characterization of the DLBCL cohort on ctDNA

The LymphGen probabilistic classification tool was used to classify DLBCL cases according to molecular clusters. A patient was assigned to a specific cluster when the tool considered the case as ''core'' or ''extended'' cluster.

3.12. Statistical analysis

The primary endpoint of the clinical study was PFS and the secondary endpoint was OS. Survival analysis was performed using the Kaplan-Meier method and compared between strata using the Log-rank test. The maximally selected rank statistics was used to identify the best cut-off values in predicting PFS for ctDNA levels and for each [^{18}F]FDG-PET/CT variable. The adjusted effects of molecular clusters, [^{18}F]FDG-PET/CT parameters and ctDNA levels on PFS and OS were estimated by Cox regression. Internal validation of the multivariate analysis was performed using the bootstrap approach with 1000 bootstrap samples. Chi square and Mann-Whitney tests were used to compare dichotomous and continuous variables, respectively. P-values were adjusted according to Benjamini-Hochberg correction. The C indices were internally validated with 1000 bootstrap samples and the means between groups were compared with the T-test. The analysis was performed with the Statistical Package for the Social Sciences (SPSS) software v.24.0 (Chicago, IL) and RStudio Version 1.2.1335 2009-2019, Inc. Statistical significance was defined as p-value < 0.05.

3. RESULTS

4.1. Patient characteristics and prognostic impact of ctDNA levels and PET/CT parameters

The cohort included 120 newly diagnosed DLBCL patients referring to our institution and homogenously treated with RCHOP- based therapy. The median age of the study cohort was 67 years, 87 (72.5%) patients presented an Ann Arbor stage III/IV and 68 (56.7%) presented an IPI ≥ 3 (Table 1). After a median follow-up of 56 months, the 40-month PFS and OS were 65.1% and 75.6%, respectively (Fig. 3A, B).

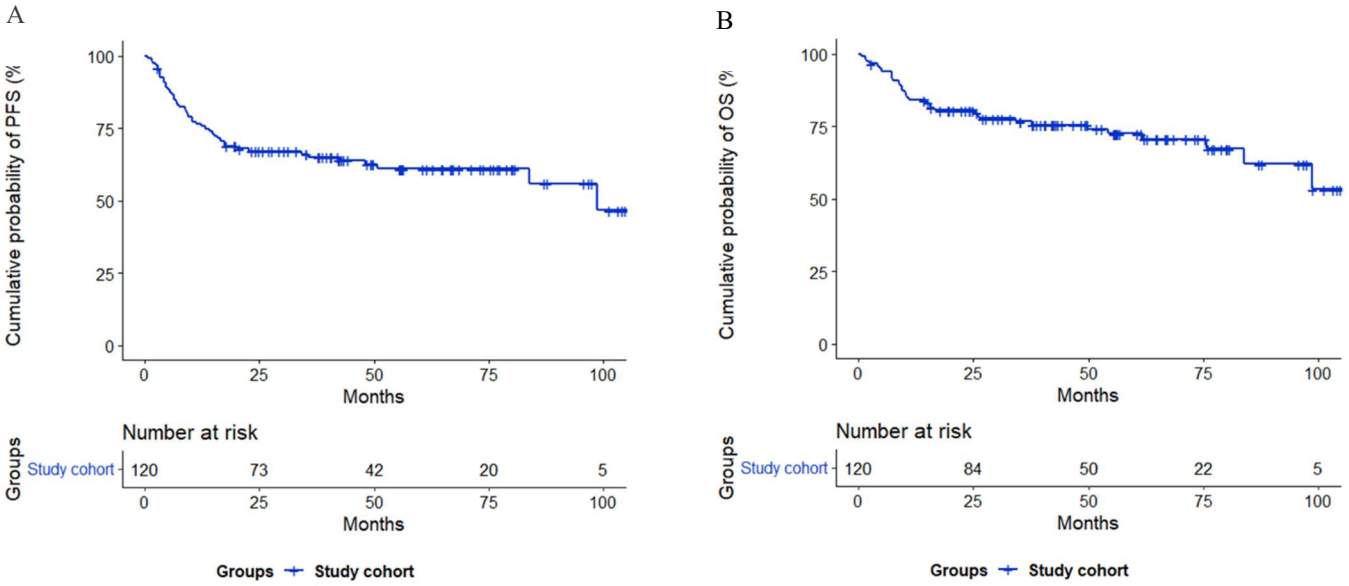

Figure 3. Kaplan-Meier curve of (A) PFS and (B) OS of the 120 DLBCL patients included in the studied cohort.

A recursive partitioning approach was used to maximize the log-rank statistics for PFS in the 120 DLBCL patients enrolled in the present study. The list of all PET/CT parameters for each individual patient is represented in Table S2. Consistently, the optimal cut-off of SUVmax, tMTV, Dmax and tTLG for predicting PFS were 17.66, 639.20 cm^3, 39 cm and 7138.34, respectively (Fig. 4A–D). For all PET/CT parameters, these cut-off values segregated patients for significantly different PFS and OS. In detail, patients with a SUVmax >17.66 (N = 78) had a 40-month PFS and OS of 57.9% and 70.5% compared to 78.6% and 84.8% for patients with a SUVmax ≤17.66 (N = 42) (p = 0.023 and p = 0.056, respectively) (Figs. 5A). Patients with a tMTV >639.20 cm^3 (N = 39) had a 40- month PFS and OS of 36.8% and 51.6% compared to 78.8% and 86.3% for patients

with a tMTV ≤639.20 cm^3 (N = 81) ($p < 0.001$ and $p = 0.0023$, respectively) (Figs. 5B). Patients with a tTLG >7138.34 (N = 33) had a 40-month PFS and OS of 34.5% and 51.0% compared to 76.7% and 84.5% for patients with a tTLG ≤7138.34 (N = 87) ($p < 0.001$ and $p = 0.0016$, respectively) (Figs. 5C). Patients with a Dmax >39 cm (N = 51) had a 40-month PFS and OS of 47.6% and 65.2% compared to 78.0% and 83.3% for patients with a Dmax ≤39 cm (N = 69) ($p = 0.018$ and $p = 0.082$, respectively (Figs. 5D).

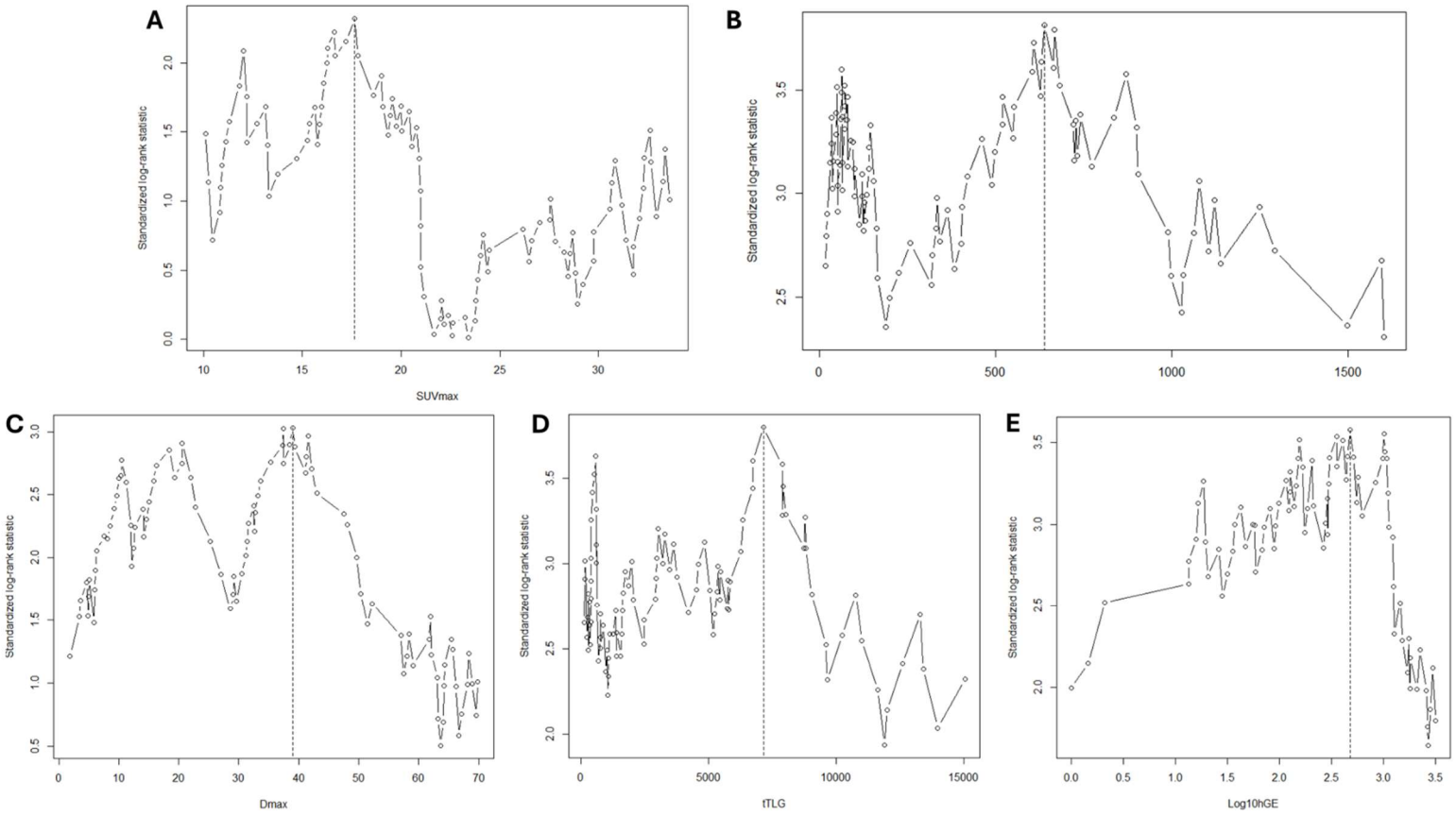

Figure 4. Maximally selected rank statistics plots. Maximally selected rank statistics plots with the best cut-off values for PFS of (**A**) SUVmax, (**B**) tMTV, (**C**) tTLG, (**D**) Dmax and (**E**) ctDNA levels.

By using the same approach utilized for PET/CT parameters, a threshold of 2.68 Log10hGE was identified as the optimal cut-off that maximizes the log-rank statistics for PFS (Fig. 4E). The complete list of variants identified on ctDNA, of ctDNA levels and of CNVs for each patient are reported in Tables S3 and S4. Patients with ctDNA levels >2.68 Log_{10}hGE (N = 43), termed ctDNA-high, had a 40-month PFS and OS of 42.9% and 55.4% compared to 77.4%

and 86.5% for ctDNA-low patients ($p < 0.001$ and $p < 0.001$, respectively) (Fig. 7A, B). The C-index based on ctDNA levels was 0.630 for PFS and 0.648 for OS (Table 2).

Table 1. Patient characteristics.

Characteristics	Values
Median Age	67 years (IQR 51–76)
Gender	
Male	50 (41.7%)
Female	70 (58.3%)
Stage	
I–II	33 (27.5%)
III–IV	87 (72.5%)
IPI	
0–1	32 (26.7%)
2	20 (16.7%)
3	33 (27.5%)
4–5	35 (29.1%)
CNS-IPI	
0–1	32 (26.7%)
2	19 (15.8%)
3	29 (24.2%)
4–5	40 (33.3%)
COO	
GC	40 (33.3%)
Non-GC	72 (60.0%)
Not available	8 (6.7%)
LDH above ULN	
Yes	69 (57.5%)
No	51 (42.5%)
Extranodal sites	
Yes	66 (55.0%)
No	54 (45.0%)
Double-expressor lymphoma	
Yes	30 (25.0%)
No	47 (39.2%)
Not available	43 (35.8%)

CNS-IPI (central nervous system) international prognostic index, *COO* cell of origin according to the Hans algorithm, GC germinal center, *LDH* lactate dehydrogenase, *ULN* upper limit of normal.

4.2. Correlations of PET/CT parameters and ctDNA levels with baseline clinical characteristics

The correlations between PET/CT variables and clinical or biological features, namely IPI score, Ann Arbor stage, cell of origin (COO), LDH, extranodal involvement and molecular clusters identified on ctDNA (A53, BN2, EZB, MCD, ST2) (Wright *et al.,* 2020), were investigated and p-values were adjusted for Benjamini-Hochberg correction. A high tMTV directly correlated with an advanced Ann Arbor stage ($p = 0.005$), elevated LDH level ($p < 0.001$), and a higher IPI score ($p = 0.004$). Higher values of tTLG directly correlated with an advanced Ann Arbor stage ($p = 0.022$),

elevated LDH level ($p < 0.001$), and a higher IPI score ($p = 0.016$). Finally, values of Dmax greater than the respective cut-off directly correlated with an advanced Ann Arbor stage ($p < 0.001$) and a higher IPI score ($p < 0.001$) (Fig. 5E).

Higher ctDNA levels directly correlated with an advanced Ann Arbor stage ($p = 0.016$), elevated LDH level ($p < 0.001$), a higher IPI score ($p = 0.049$), MCD cluster ($p = 0.030$) and BN2 cluster ($p = 0.016$) (Fig. 5E).

Moreover, by evaluating the relationship between PET/CT variables and ctDNA levels, ctDNA levels >2.68 Log10hGE directly correlated with higher values of tMTV ($p < 0.001$), TLG ($p < 0.001$) and Dmax ($p = 0.016$), while there was not a significant correlation with higher SUVmax values (Fig. 5E).

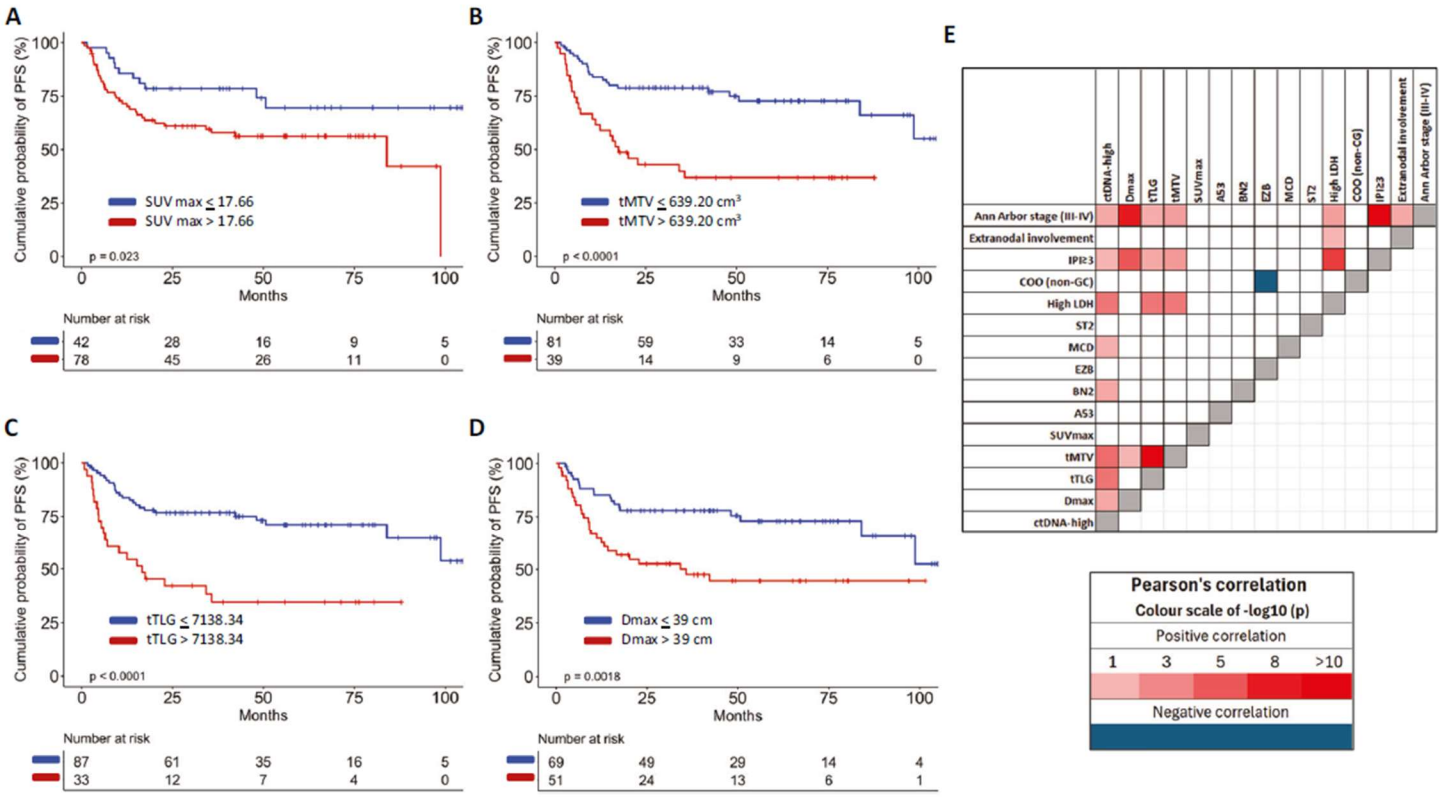

Figure 5. Prognostic impact on PFS of each PET/CT variable and clinical-molecular correlations. Kaplan-Meier estimates of PFS according to cut-off values of (**A**) SUVmax, (**B**) tMTV, (**C**) tTLG and (**D**) Dmax. Patients with values under the respective cut-off for each PET/CT parameter are represented by the blue curves and patients above the cut-off are represented by the red curves. **E** Correlation map comparing clinical, metabolic and molecular features. The red color scale of -log10 (p) points to a co-occurrence between two variables. The blue color scale of -log10 (p) points to a mutual exclusivity between two variables. The intensity of the color corresponds to the strength of the correlation. The white boxes denote non-significant correlations.

4.3. Integration between ctDNA levels and PET/CT parameters

After assessing the individual prognostic impact of ctDNA levels and each PET/CT parameter, we proceeded to investigate whether their integration would improve outcome prediction. In four different bivariate Cox regression analyses including each single PET/CT feature together with ctDNA levels, tMTV (HR 2.42, 95% CI 1.28-4.58, p = 0.007), tTLG (HR 2.42, 95% CI 1.28-4.60, p = 0.007) and Dmax (HR 1.97, 95% CI 1.07-3.65, p = 0.031) maintained an independent association with a shorter PFS, while SUVmax (HR 1.84, 95% CI 0.91-3.69, p = 0.087) lost its prognostic value (Fig. 6A–D). In all the above-mentioned bivariate analyses, ctDNA levels also retained independent association with shorter PFS (Fig. 6A–D). Therefore, patients with at least one PET/CT value (namely tMTV, tTLG or Dmax) above the respective cut-off were grouped as high-risk PET patients (N = 67). More precisely, 18 patients have all the three PET/CT variables above the respective cut-off, 20 patients have two PET/CT variables above the respective cut-off and 29 patients have only one PET/CT variable above the respective cut-off. High-risk PET patients had a significantly worse outcome compared to low-risk PET patients, with a 40-month PFS and OS of 45.4% and 62.2% compared to 90.4% and 92.3% (p < 0.001 and p = 0.007, respectively) (Fig. 7C, D). The C-index for the high-risk PET variable was 0.685 for PFS and 0.645 for OS (Table 2).

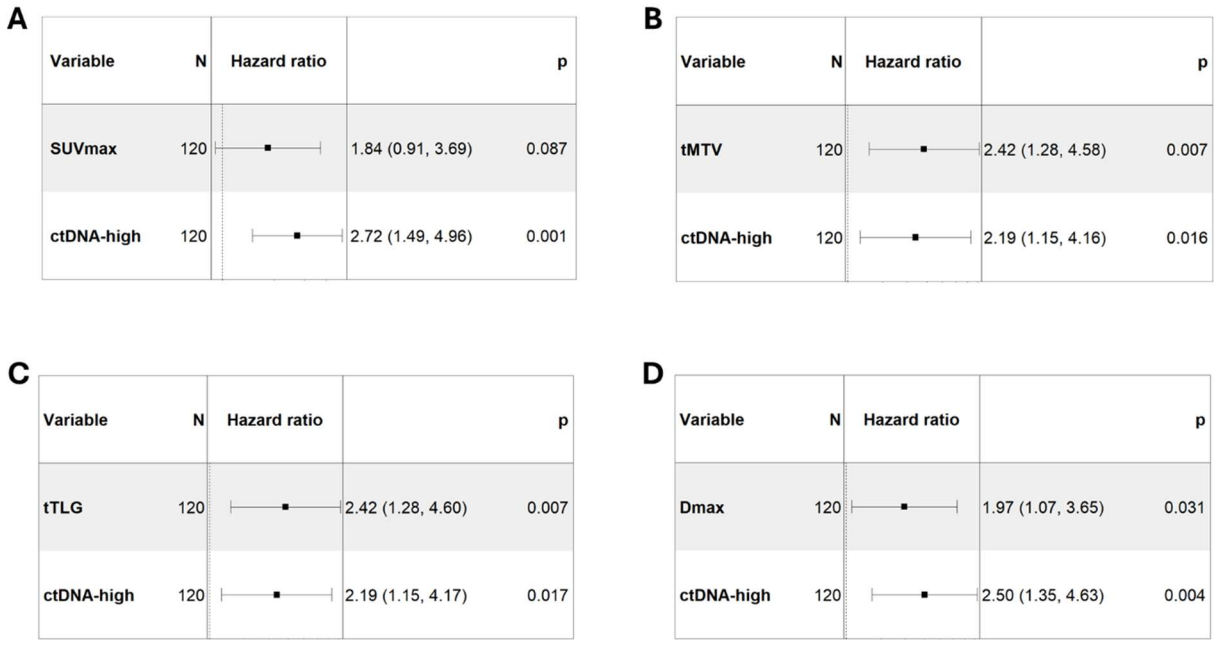

Figure 6. Prognostic impact of each PET/CT variable adjusted for ctDNA-levels. Multivariate analysis of PFS including (**A**) SUVmax, (**B**) tMTV, (**C**) tTLG and (**D**) Dmax and ctDNA levels > 2.68 log hGE/mL.

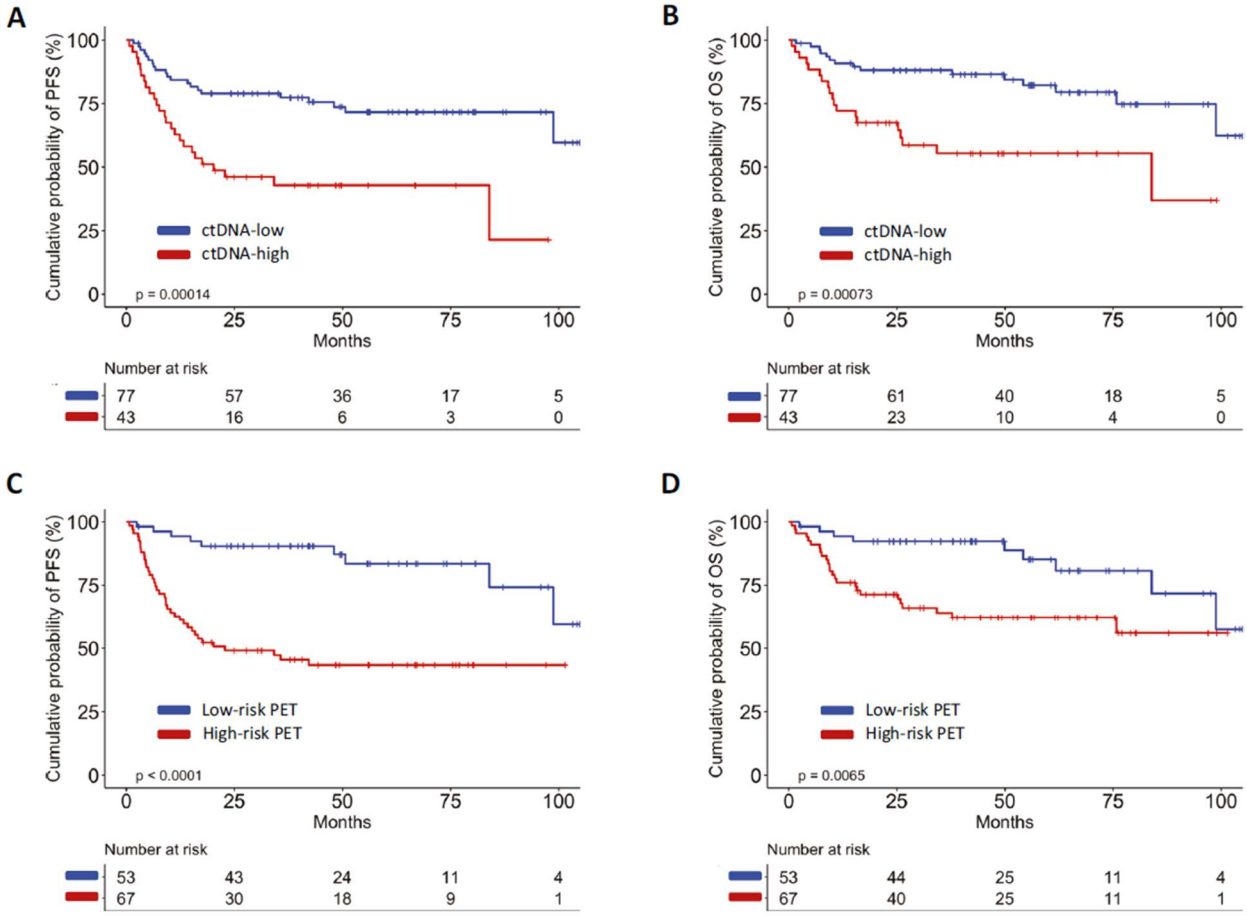

Figure 7. Prognostic impact of ctDNA-high and high-risk PET variables. Kaplan-Meier estimates of (**A**) PFS and (**B**) OS according to ctDNA levels. Patients with ctDNA levels ≤ 2.68 log hGE/mL are represented by the blue curves and patients with ctDNA levels > 2.68 log hGE/mL are represented by the red curves. Kaplan-Meier estimates of (**C**) PFS and (**D**) OS according to the presence of at least one PET/CT variable above the respective cut-off value (high-risk PET). Low-risk PET patients are represented by the blue curves and high-risk PET patients are represented by the red curves.

By multivariate analysis, ctDNA-high (HR 2.04, 95% CI 1.10-3.78, p = 0.024) and high-risk PET (HR 3.84, 95% CI 1.78-8.28, p < 0.001) independently predicted PFS (Fig. 8A). Relying on β coefficients, 1 point was assigned to ctDNA-high patients and 2 points were assigned to high-risk PET patients. Patients were then grouped into three risk classes, according to their total score, and presented significantly different outcomes (p < 0.001 for both PFS and OS). Low-risk DLBCL (0 points, N = 44) were both ctDNAlow and low-risk PET and presented a 40-month PFS and OS of 93.0% and 95.3%. Intermediate-risk DLBCL (1 and 2 points, N = 42) were either ctDNA-high or high-risk PET and presented a 40- month PFS and OS of 61.5% and 75.4%. High-risk DLBCL

(3 points, N = 34) were both ctDNA-high and high-risk PET and presented a 40-month PFS and OS of 33.6% and 49.8% (Fig. 8B, C). Importantly, when compared to ctDNA-high and high-risk PET variables alone, the novel 2-factor prognostic model improved the C-index for both PFS and OS (0.712 and 0.696, respectively) (Table 2).

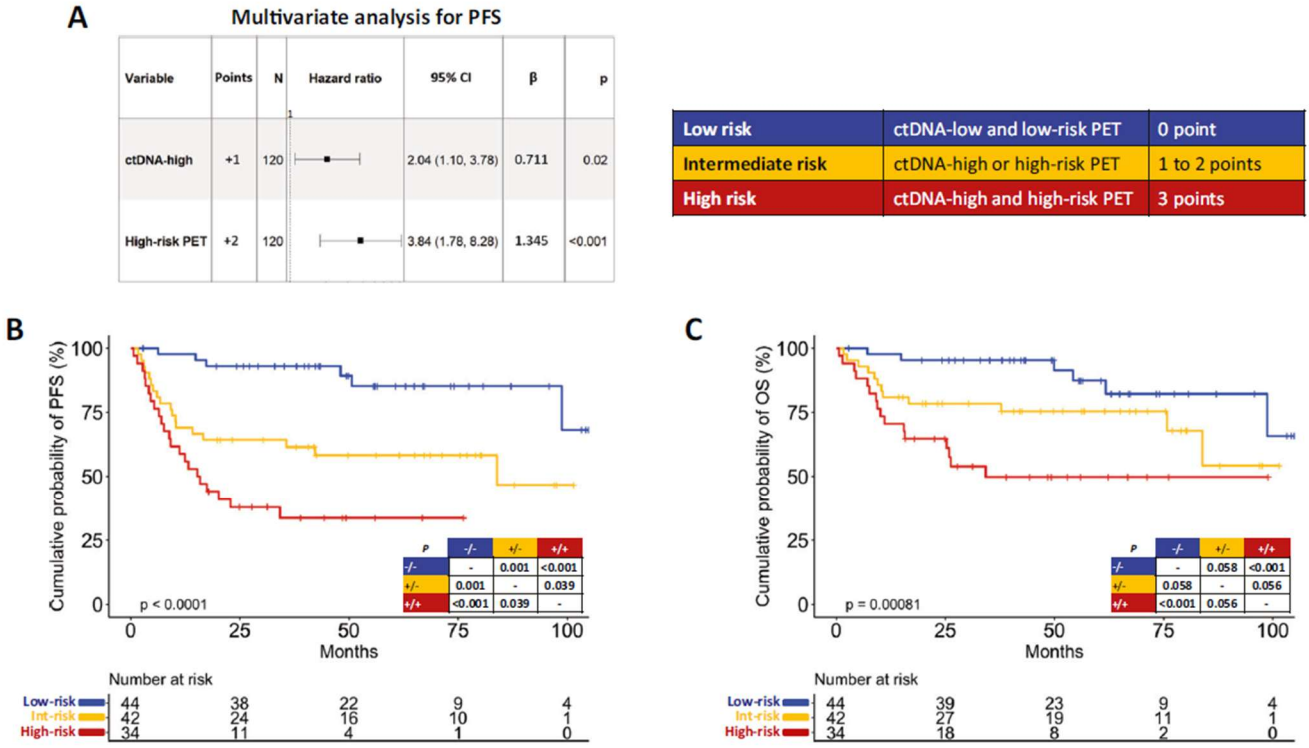

Figure 8. Integration between ctDNA levels and PET/CT into the 2-factor prognostic model. A Multivariate analysis of PFS including ctDNAhigh and high-risk PET variables with β coefficients and points assigned to each variable. The table shows how the patients were grouped based on their total score. Kaplan-Meier estimates of (**B**) PFS and (**C**) OS according to the two-variable score. Low-risk patients (0 points, both ctDNA-low and low-risk PET) are represented by the blue curves, intermediate-risk patients (1 and 2 points, either ctDNA-high or high-risk PET) are represented by the yellow curves, high-risk patients (3 points, both ctDNA high and high-risk PET) are represented by the red curves.

Table 2. C-indices for PFS and OS of the proposed prognostic models.

Prognostic model	C-index for PFS	C-index for OS
ctDNA-high	0.630	0.648
High-risk PET	0.685	0.645
ctDNA + high-risk PET (2-factor model)	0.712	0.696
ctDNA + high-risk PET + BN2/EZB/ST2 (3-factor model)	0.745	0.746

4.4. Molecular clusters on liquid biopsy improve outcome prediction

Since molecular clusters identified on liquid biopsy harbor prognostic relevance in DLBCL patients (Moia *et al.,* 2025), we tried to integrate this biological feature into the 2-factor prognostic score. As expected, A53 (40-month PFS 0%) and MCD (40-month PFS 33.3%) clusters were associated with a worse outcome, whereas patients belonging to BN2 (40-month PFS 83.3%), EZB (40-month PFS 83.3%) or ST2 (40-month PFS 75.0%) clusters were associated with a better outcome after R-CHOP (Fig. 9A, B). By combining the molecular clusters associated with favorable outcomes (BN2, EZB and ST2 clusters; N = 33), patients belonging to this group presented a 40-month PFS and OS of 81.3% and 90.0% compared to 59.3% and 70.3% for patients belonging to other molecular clusters or not classified (N = 87) (p = 0.044 and p = 0.028, respectively) (Fig. 9C, D).

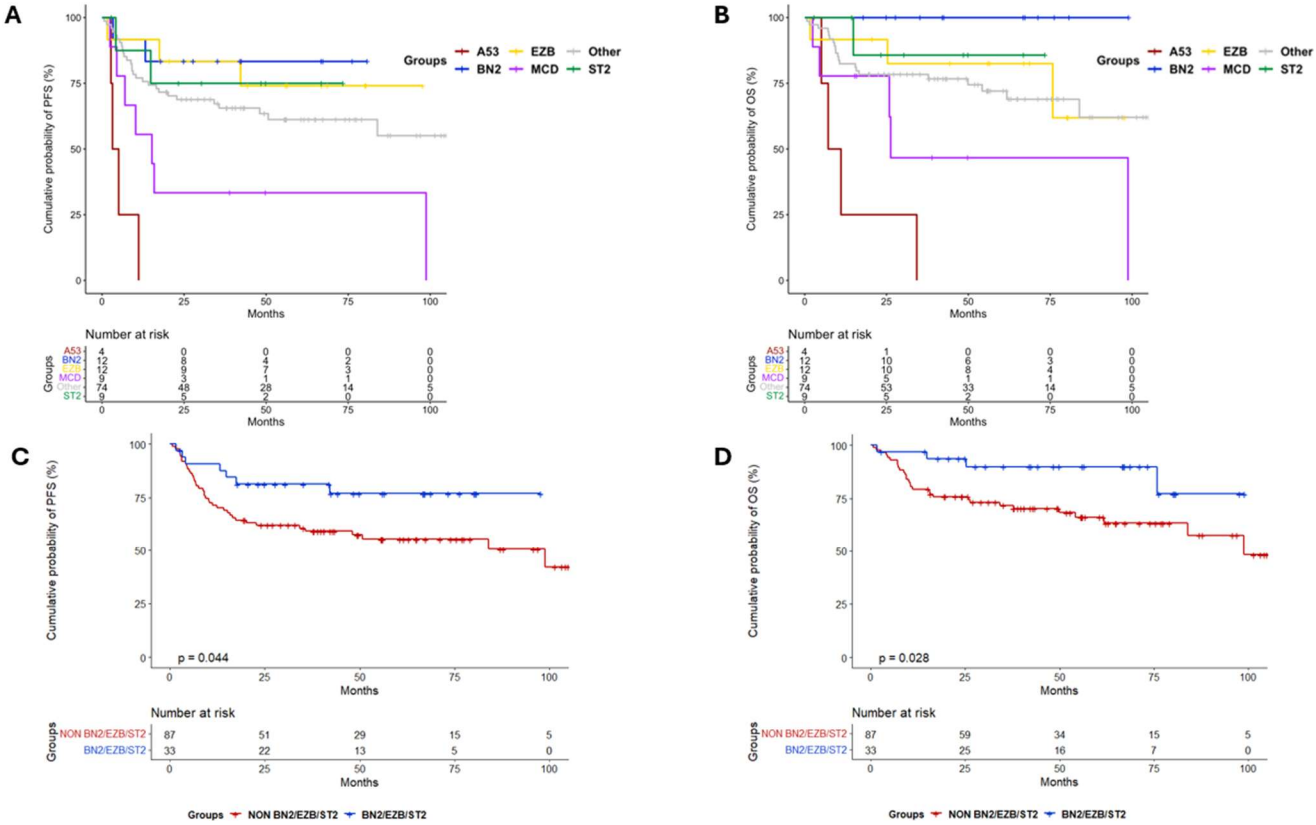

Figure 9. Prognostic impact of molecular cluster on ctDNA. Kaplan-Meier estimates of **(A)** PFS and **(B)** OS according to molecular cluster classification. Patients assigned to A53 cluster are represented by the red curves, patients assigned to BN2 cluster by the blue curves, patients assigned to EZB cluster by the yellow curves, patients assigned to MCD cluster by the pink curves, patients assigned to ST2 cluster by the green curves and patients not assigned to any molecular cluster are represented by the grey curves. Kaplan-Meier estimates of **(C)** PFS and **(D)** OS according to BN2/EZB/ST2 molecular cluster assignment. Patients assigned to BN2/EZB/ST2 clusters are represented by the blue curves and patients not assigned to BN2/EZB/ST2 clusters are represented by the red curves.

In multivariate analysis, BN2/EZB/ST2 clusters (HR 0.27, 95% CI 0.12-0.62, p = 0.02) maintained an independent association with a better PFS even when adjusted for ctDNA-high (HR 2.77, 95% CI 1.45-5.27, p = 0.002) and for high-risk PET (HR 3.90, 95% CI 1.79- 8.48, p < 0.001) (Fig. 10A).

A novel 3-factor prognostic model was therefore devised. According to the β coefficients, 1 point was assigned to ctDNAhigh, 1.5 points to high-risk PET and −1.5 points to BN2/EZB/ST2 patients. Three different groups with unique PFS and OS were identified. Low-risk DLBCL (−1.5 to 0.5 points, N = 57) presented a 40-month PFS and OS of 91.1% and 94.6%, intermediate-risk DLBCL (1 to 1.5 points, N = 41) presented a 40-month PFS and OS of 58.1% and 74.6%, and high-risk DLBCL (2.5 points, N = 22) presented a 40-month PFS and OS of 12.1% and 27.3%, respectively (both p < 0.001) (Fig. 10B, C). Notably, the variables of the 3-factor prognostic model were all frequently selected by internal 1000X bootstrap validation (bootstrap selection ranging from 85.0% to 96.4%; Fig. 8A). Importantly, when compared to the previous 2-factor prognostic model, the addition of molecular clusters into the 3-factor prognostic model significantly improved, after internal 1000X bootstrap validation, the C-statistics both for PFS (mean C-index 0.745, 95% CI 0.668- 0.799, p < 0.0001) and for OS (mean C-index 0.746, 95% CI 0.649-0.813, p < 0.0001) (Table 2). Also, eight random training-validation splits of the dataset using 80 patients as training and 40 patients as validation were performed. In all 8 iterations, the progression-free survival curves of the 3-factor prognostic model maintained statistical significance.

Finally, the variables of the 3-factor prognostic model were compared with the prognostic markers currently used in the clinical practice to predict outcome in newly diagnosed DLBCL, namely IPI and COO. In multivariate analysis, both IPI ≥ 3 (HR 0.85, 95% CI 0.41–1.76, p = 0.662) and non-GC COO (HR 1.58, 95% CI 0.72–3.47, p = 0.259) lost their prognostic impact, whereas ctDNAhigh (HR 2.45, 95% CI 1.22–4.96, p = 0.012) and a high-risk PET (HR 6.50, 95% CI 2.38–18.03, p < 0.001) maintained an independent association with a shorter PFS and BN2/EZB/ST2 clusters (HR 0.32, 95% CI 0.13–0.83, p = 0.020) maintained an independent association with a better PFS (Table 3).

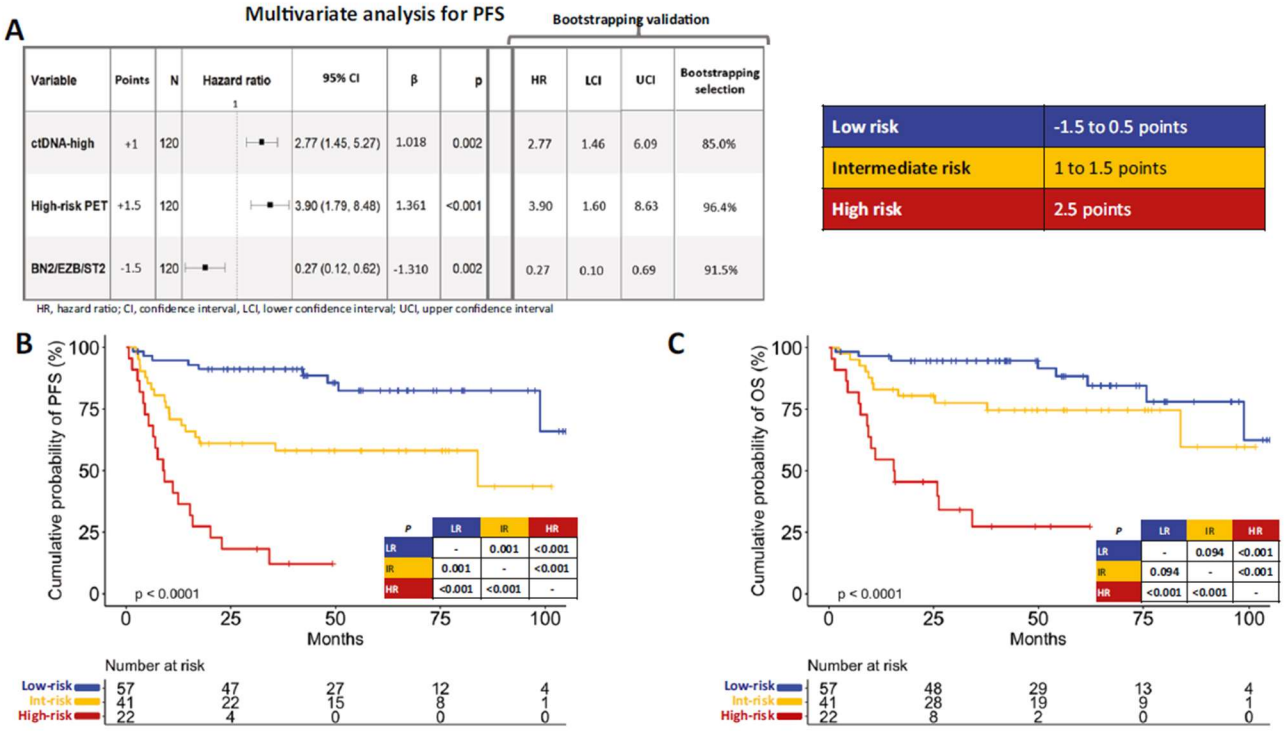

Figure 10. Integration between ctDNA levels, PET/CT and molecular clusters into the 3-factor prognostic model. A Multivariate analysis with bootstrapping validation of PFS including ctDNA-high, high-risk PET and BN2/EZB/ST2 variables with β coefficients and points assigned to each variable. The table shows how the patients were grouped based on their total score. Kaplan-Meier estimates of (**B**) PFS and (**C**) OS according to the three-variable score. Low-risk patients (−1.5 to 0.5 points) are represented by the blue curves, intermediate-risk patients (1–1.5 points) are represented by the yellow curves, high-risk patients (2.5 points) are represented by the red curves.

Table 3. Multivariate analysis comparing ctDNA-high, high-risk PET, BN2/EZB/ST2 clusters, IPI and COO in terms of PFS.

Variable	*p*	HR	95% CI
ctDNA-high	0.012	2.46	1.22–4.96
High-risk PET	<0.001	6.55	2.38–18.03
BN2/EZB/ST2	0.020	0.33	0.13–0.84
IPI ≥ 3	0.662	0.85	0.41–1.76
COO (non-GC)	0.259	1.58	0.71–3.47

5. DISCUSSION

The present study employed a multilayered approach integrating three distinct prognostic markers for DLBCL - i.e. PET/CT radiomics, ctDNA levels, and molecular clusters from liquid biopsy - into a novel 3-factor prognostic model that stratifies patient outcomes with a greater accuracy than clinical prognostic biomarkers.

Different PET/CT radiomics features have been demonstrated capable of predicting outcomes in DLBCL (Cottereau et al., 2020; Frood et al., 2021; Mikhaeel et al., 2022; Zhang et al., 2019). The bidimensional parameters, i.e. SUVmax, have an established prognostic value, but the tridimensional parameters, namely tMTV, tTLG and Dmax, may capture also spatial heterogeneity and disease dissemination(Cottereau et al., 2020; Frood et al., 2021).Various approaches have been employed to assess the prognostic impact of tMTV, tTLG and Dmax, considering them as either continuous or dichotomic variables. However, no clear cut-off has been established to date, due to heterogeneity across studies in the cut-off values, which largely depends on the study population, software platforms for analysis, and statistical approaches adopted (Ceriani et al., 2025; Eertink et al., 2022; Mikhaeel et al., 2022; Sasanelli et al., 2014; Vercellino et al., 2020; Zhang et al., 2019). To ensure consistent analysis of all available data, this study employed the maximally selected rank statistics to determine the optimal cut-off values to predict PFS for each PET/CT variable. The cut-off values identified in this study need further validation in additional DLBCL patient cohorts to confirm their prognostic significance and their potential for implementation in the clinical practice.

In order to test the independent prognostic value of each PET/CT parameter with ctDNA levels, max-stat statistics was also applied to ctDNA levels and the 2.68 log hGE/mL cut-off (very close to the previously reported value of 2.5 log hGE/mL) (Kurtz et al., 2018). was identified as the optimal value to predict DLBCL outcome. Importantly, in the multivariate analysis of the 3-factor prognostic model, use of the 2.5 log hGE/mL cut-off allowed to achieve superimposable outcome results. Subsequently, by multivariate analysis, the tridimensional PET/CT parameters (i.e. tMTV, tTLG and Dmax) retained their prognostic significance after adjustment for ctDNA levels, whereas the bidimensional PET/CT parameter SUVmax lost its prognostic impact. This finding highlights the importance of capturing the anatomical heterogeneity of DLBCL by considering the potential impact of all individual lesions identified during PET/CT staging (by

using tMTV, tTLG and Dmax), rather than focusing solely on the most metabolically active lesion (by using SUVmax). Therefore, patients with at least one PET/CT parameter among tMTV, tTLG and Dmax above the respective cut-off value were grouped as high-risk PET patients.

An early identification of relapsing/refractory DLBCL patients a priori before re-treatment represents a major unmet clinical need. To address this issue, we integrated the three prognostic markers investigated in this cohort, namely PET/CT parameters (tMTV, tTLG and Dmax), ctDNA levels and molecular clusters. Initially, the 2-factor prognostic model validated the independent prognostic value of high-risk PET and ctDNA-high levels. However, PET/CT scans and ctDNA levels merely represent a phenotypic expression of an underlying molecular landscape, that varies among patients and influences their clinical presentation.

To address the molecular heterogeneity of DLBCL, we took advantage of the recent demonstration that ctDNA analysis with the LymphGen tool allows to classify a fraction of DLBCL into distinct molecular clusters, thereby providing insights into the intrinsic disease biology (Moia et al., 2025; Wright et al., 2020). Importantly, the molecular profiles and outcomes of the clusters identified in this study were consistent with previous findings. For instance, the A53 cluster showed an enrichment of CNVs compared to non A53 patients ($p = 0.038$) and the MCD cluster was associated with poor outcomes (Wright et al., 2020). Notably, the percentage of classified patients in our cohort (i.e. 38.4%) is in line with previous studies using targeted panels and classifying approximately 40% of patients (Rivas-Delgado et al., 2021). In the current cohort, both the proportion of classifiable patients and the clinical impact of the clusters identified on ctDNA closely mirrored those observed on the tissue biopsy.

The greatest improvement in outcome prediction documented by C-statistics was achieved by incorporating molecular clusters into the 3-factor prognostic model, further supporting the notion that the underlying DLBCL biology enhances outcome prediction. Previous studies have investigated the integration of liquid biopsy with PET/CT, but they included only one liquid biopsy biomarker (i.e. ctDNA levels) with only one PET/CT parameter (i.e. tMTV) (Dean et al., 2023). To the best of our knowledge, this study is the first to demonstrate that multiple PET/CT parameters (i.e. tMTV, tTLG and Dmax) and multiple liquid biopsy biomarkers (i.e. ctDNA levels and molecular clusters), if integrated simultaneously into a single prognostic score, significantly improve DLBCL outcome prediction compared to using each biomarker individually. Importantly,

the variables of the 3-factor prognostic model outperformed the prognostic impact of clinical parameters routinely used in the clinical practice, namely IPI and COO.

This study aimed at demonstrating the feasibility of integrating liquid biopsy with PET/CT parameters, rather than validating a specific prognostic score. Based on sample power analysis, a single cohort of at least 114 DLBCL patients was required to demonstrate that, compared to ctDNA levels only, the integration of PET/CT parameters, ctDNA levels and molecular clusters can improve this sensitivity in predicting cure from 72.5% to 85% (assuming a type I error rate of $\alpha = 0.05$ and 90% power)(Kurtz et al., 2018). Accordingly, a training-validation design was not employed, and all 120 DLBCL patients were included in the analysis. Nevertheless, to mitigate the lack of an external validation, we have performed extensive internal validation through multiple bootstrapping analyses and all retained statistical significance.

The present study also provides the background for dynamic investigations of the multilayered biomarker assessment utilized herein. In fact, in addition to the static baseline evaluation at diagnosis, monitoring the dynamic changes in ctDNA levels and PET/CT parameters during treatment and at therapy completion might offer potential valuable prognostic insights. This approach may help anticipate disease progression or early relapse, even when traditional radiologic and metabolic assessments based on the Lugano criteria suggest a favorable response (Soscia et al., 2024). Notably, recent evidence has documented that molecular clusters identified at diagnosis on the tissue biopsy enhance the prognostic accuracy of end-of-therapy (EOT) PET/CT when solely based on the Deauville score(Mendeville et al., 2025).

Liquid biopsy biomarkers are minimally invasive and capture information from all disease sites, and PET/CT scans are already used for staging and evaluating response assessment in DLBCL. The assessment of these prognostic markers in the clinical practice and combining them in a prognostic score is devoid of major hurdles for patients, appears to be feasible, and might help identify DLBCL patients who may benefit most from standard chemoimmunotherapy, as well as cases at high risk of early relapse who should be prioritized for the access to innovative treatment strategies. Dedicated clinical trials combining liquid biopsy biomarkers with PET/CT parameters during the first cycle of standard chemoimmunotherapy might be pivotal to identify high-risk DLBCL patients who may benefit the most from an early switch to bispecific monoclonal antibodies and/or CAR-T cell therapy.

REFERENCES

Alig, S., Macaulay, C. W., Kurtz, D. M., Dührsen, U., Hüttmann, A., Schmitz, C., Jin, M. C., Sworder, B. J., Garofalo, A., Shahrokh Esfahani, M., Nabet, B. Y., Soo, J., Scherer, F., Craig, A. F. M., Casasnovas, O., Westin, J. R., Gaidano, G., Rossi, D., Roschewski, M., … Alizadeh, A. A. (2021). Short Diagnosis-to-Treatment Interval Is Associated With Higher Circulating Tumor DNA Levels in Diffuse Large B-Cell Lymphoma. *Journal of Clinical Oncology*, *39*(23), 2605–2616. https://doi.org/10.1200/JCO.20.02573

Alizadeh, A. A., Eisen, M. B., Davis, R. E., Ma, C., Lossos, I. S., Rosenwald, A., Boldrick, J. C., Sabet, H., Tran, T., Yu, X., Powell, J. I., Yang, L., Marti, G. E., Moore, T., Hudson, J., Lu, L., Lewis, D. B., Tibshirani, R., Sherlock, G., … Staudt, L. M. (2000). Distinct types of diffuse large B-cell lymphoma identified by gene expression profiling. *Nature*, *403*(6769), 503–511. https://doi.org/10.1038/35000501

Almasri, M., Maher, N., Al Deeban, B., Diop, N. M., Moia, R., & Gaidano, G. (2025). Liquid Biopsy in B and T Cell Lymphomas: From Bench to Bedside. *International Journal of Molecular Sciences*, *26*(10), 4869. https://doi.org/10.3390/ijms26104869

Barrans, S., Crouch, S., Smith, A., Turner, K., Owen, R., Patmore, R., Roman, E., & Jack, A. (2010). Rearrangement of *MYC* Is Associated With Poor Prognosis in Patients With Diffuse Large B-Cell Lymphoma Treated in the Era of Rituximab. *Journal of Clinical Oncology*, *28*(20), 3360–3365. https://doi.org/10.1200/JCO.2009.26.3947

Barrans, S. L., Evans, P. A. S., O'Connor, S. J. M., Kendall, S. J., Owen, R. G., Haynes, A. P., Morgan, G. J., & Jack, A. S. (2003). The t(14;18) is associated with germinal center-derived diffuse large B-cell lymphoma and is a strong predictor of outcome. *Clinical Cancer Research: An Official Journal of the American Association for Cancer Research*, *9*(6), 2133–2139.

Barrington, S. F., & Meignan, M. (2019). Time to Prepare for Risk Adaptation in Lymphoma by Standardizing Measurement of Metabolic Tumor Burden. *Journal of Nuclear Medicine*, *60*(8), 1096–1102. https://doi.org/10.2967/jnumed.119.227249

Basso, K., & Dalla-Favera, R. (2015). Germinal centres and B cell lymphomagenesis. *Nature Reviews Immunology*, *15*(3), 172–184. https://doi.org/10.1038/nri3814

Bereshchenko, O. R., Gu, W., & Dalla-Favera, R. (2002). Acetylation inactivates the transcriptional repressor BCL6. *Nature Genetics*, *32*(4), 606–613. https://doi.org/10.1038/ng1018

Boice, M., Salloum, D., Mourcin, F., Sanghvi, V., Amin, R., Oricchio, E., Jiang, M., Mottok, A., Denis-Lagache, N., Ciriello, G., Tam, W., Teruya-Feldstein, J., De Stanchina, E., Chan, W. C., Malek, S. N., Ennishi, D., Brentjens, R. J., Gascoyne, R. D., Cogné, M., … Wendel, H.-G. (2016). Loss of the HVEM Tumor Suppressor in Lymphoma and Restoration by Modified CAR-T Cells. *Cell*, *167*(2), 405-418.e13. https://doi.org/10.1016/j.cell.2016.08.032

Boone, D. L., Turer, E. E., Lee, E. G., Ahmad, R.-C., Wheeler, M. T., Tsui, C., Hurley, P., Chien, M., Chai, S., Hitotsumatsu, O., McNally, E., Pickart, C., & Ma, A. (2004). The ubiquitin-modifying enzyme A20 is required for termination of Toll-like receptor responses. *Nature Immunology*, *5*(10), 1052–1060. https://doi.org/10.1038/ni1110

Burotto, M., Berkovits, A., & Dunleavy, K. (2016). Double hit lymphoma: From biology to therapeutic implications. *Expert Review of Hematology*, *9*(7), 669–678. https://doi.org/10.1080/17474086.2016.1182858

Carreras, J., Lopez-Guillermo, A., Kikuti, Y. Y., Itoh, J., Masashi, M., Ikoma, H., Tomita, S., Hiraiwa, S., Hamoudi, R., Rosenwald, A., Leich, E., Martinez, A., Roncador, G., Villamor, N., Colomo, L., Perez, P., Tsuji, N. M., Campo, E., & Nakamura, N. (2019). High TNFRSF14 and low

BTLA are associated with poor prognosis in Follicular Lymphoma and in Diffuse Large B-cell Lymphoma transformation. *Journal of Clinical and Experimental Hematopathology*, *59*(1), 1–16. https://doi.org/10.3960/jslrt.19003

Cattoretti, G., Mandelbaum, J., Lee, N., Chaves, A. H., Mahler, A. M., Chadburn, A., Dalla-Favera, R., Pasqualucci, L., & MacLennan, A. J. (2009). Targeted Disruption of the *S1P 2* Sphingosine 1-Phosphate Receptor Gene Leads to Diffuse Large B-Cell Lymphoma Formation. *Cancer Research*, *69*(22), 8686–8692. https://doi.org/10.1158/0008-5472.CAN-09-1110

Ceriani, L., Milan, L., Chauvie, S., & Zucca, E. (2025). Understandings 18 FDG PET radiomics and its application to lymphoma. *British Journal of Haematology*, *206*(6), 1546–1559. https://doi.org/10.1111/bjh.20074

Challa-Malladi, M., Lieu, Y. K., Califano, O., Holmes, A. B., Bhagat, G., Murty, V. V., Dominguez-Sola, D., Pasqualucci, L., & Dalla-Favera, R. (2011). Combined Genetic Inactivation of β2-Microglobulin and CD58 Reveals Frequent Escape from Immune Recognition in Diffuse Large B Cell Lymphoma. *Cancer Cell*, *20*(6), 728–740. https://doi.org/10.1016/j.ccr.2011.11.006

Chapuy, B., Stewart, C., Dunford, A. J., Kim, J., Kamburov, A., Redd, R. A., Lawrence, M. S., Roemer, M. G. M., Li, A. J., Ziepert, M., Staiger, A. M., Wala, J. A., Ducar, M. D., Leshchiner, I., Rheinbay, E., Taylor-Weiner, A., Coughlin, C. A., Hess, J. M., Pedamallu, C. S., … Shipp, M. A. (2018). Molecular subtypes of diffuse large B cell lymphoma are associated with distinct pathogenic mechanisms and outcomes. *Nature Medicine*, *24*(5), 679–690. https://doi.org/10.1038/s41591-018-0016-8

Chapuy, B., Wood, T., Stewart, C., Dunford, A., Wienand, K., Khan, S. J., Serin, N., Wang, M., Calabretta, E., Shimono, J., Van Seters, S., Wisemann, S., Belkin, S., Heimann, D., Redd, R.,

Shipp, M. A., & Getz, G. (2025a). DLB *class*: A probabilistic molecular classifier to guide clinical investigation and practice in diffuse large B-cell lymphoma. *Blood*, *145*(18), 2041–2055. https://doi.org/10.1182/blood.2024025652

Chapuy, B., Wood, T., Stewart, C., Dunford, A., Wienand, K., Khan, S. J., Serin, N., Wang, M., Calabretta, E., Shimono, J., Van Seters, S., Wisemann, S., Belkin, S., Heimann, D., Redd, R., Shipp, M. A., & Getz, G. (2025b). DLB *class*: A probabilistic molecular classifier to guide clinical investigation and practice in diffuse large B-cell lymphoma. *Blood*, *145*(18), 2041–2055. https://doi.org/10.1182/blood.2024025652

Chiappella, A., Tucci, A., Castellino, A., Pavone, V., Baldi, I., Carella, A. M., Orsucci, L., Zanni, M., Salvi, F., Liberati, A. M., Gaidano, G., Bottelli, C., Rossini, B., Perticone, S., De Masi, P., Ladetto, M., Ciccone, G., Palumbo, A., Rossi, G., … on behalf of the Fondazione Italiana Linfomi. (2013). Lenalidomide plus cyclophosphamide, doxorubicin, vincristine, prednisone and rituximab is safe and effective in untreated, elderly patients with diffuse large B-cell lymphoma: A phase I study by the Fondazione Italiana Linfomi. *Haematologica*, *98*(11), 1732–1738. https://doi.org/10.3324/haematol.2013.085134

Coiffier, B., & Sarkozy, C. (2016). Diffuse large B-cell lymphoma: R-CHOP failure—what to do? *Hematology*, *2016*(1), 366–378. https://doi.org/10.1182/asheducation-2016.1.366

Compagno, M., Lim, W. K., Grunn, A., Nandula, S. V., Brahmachary, M., Shen, Q., Bertoni, F., Ponzoni, M., Scandurra, M., Califano, A., Bhagat, G., Chadburn, A., Dalla-Favera, R., & Pasqualucci, L. (2009). Mutations of multiple genes cause deregulation of NF-κB in diffuse large B-cell lymphoma. *Nature*, *459*(7247), 717–721. https://doi.org/10.1038/nature07968

Cottereau, A.-S., Nioche, C., Dirand, A.-S., Clerc, J., Morschhauser, F., Casasnovas, O., Meignan, M., & Buvat, I. (2020). ^{18} F-FDG PET Dissemination Features in Diffuse Large B-Cell Lymphoma Are Predictive of Outcome. *Journal of Nuclear Medicine*, *61*(1), 40–45. https://doi.org/10.2967/jnumed.119.229450

Czermin, B., Melfi, R., McCabe, D., Seitz, V., Imhof, A., & Pirrotta, V. (2002). Drosophila Enhancer of Zeste/ESC Complexes Have a Histone H3 Methyltransferase Activity that Marks Chromosomal Polycomb Sites. *Cell*, *111*(2), 185–196. https://doi.org/10.1016/S0092-8674(02)00975-3

Davis, R. E., Ngo, V. N., Lenz, G., Tolar, P., Young, R. M., Romesser, P. B., Kohlhammer, H., Lamy, L., Zhao, H., Yang, Y., Xu, W., Shaffer, A. L., Wright, G., Xiao, W., Powell, J., Jiang, J., Thomas, C. J., Rosenwald, A., Ott, G., … Staudt, L. M. (2010). Chronic active B-cell-receptor signalling in diffuse large B-cell lymphoma. *Nature*, *463*(7277), 88–92. https://doi.org/10.1038/nature08638

De Silva, N. S., & Klein, U. (2015). Dynamics of B cells in germinal centres. *Nature Reviews Immunology*, *15*(3), 137–148. https://doi.org/10.1038/nri3804

Dean, E. A., Kimmel, G. J., Frank, M. J., Bukhari, A., Hossain, N. M., Jain, M. D., Dahiya, S., Miklos, D. B., Altrock, P. M., & Locke, F. L. (2023). Circulating tumor DNA adds specificity to PET after axicabtagene ciloleucel in large B-cell lymphoma. *Blood Advances*, *7*(16), 4608–4618. https://doi.org/10.1182/bloodadvances.2022009426

Dominguez-Sola, D., Kung, J., Holmes, A. B., Wells, V. A., Mo, T., Basso, K., & Dalla-Favera, R. (2015). The FOXO1 Transcription Factor Instructs the Germinal Center Dark Zone Program. *Immunity*, *43*(6), 1064–1074. https://doi.org/10.1016/j.immuni.2015.10.015

Dunleavy, K., & Wilson, W. H. (2014). Appropriate management of molecular subtypes of diffuse large B-cell lymphoma. *Oncology (Williston Park, N.Y.)*, *28*(4), 326–334.

Eertink, J. J., Van De Brug, T., Wiegers, S. E., Zwezerijnen, G. J. C., Pfaehler, E. A. G., Lugtenburg, P. J., Van Der Holt, B., De Vet, H. C. W., Hoekstra, O. S., Boellaard, R., & Zijlstra, J. M. (2022). 18F-FDG PET baseline radiomics features improve the prediction of treatment outcome in diffuse large B-cell lymphoma. *European Journal of Nuclear Medicine and Molecular Imaging*, *49*(3), 932–942. https://doi.org/10.1007/s00259-021-05480-3

Frood, R., Burton, C., Tsoumpas, C., Frangi, A. F., Gleeson, F., Patel, C., & Scarsbrook, A. (2021). Baseline PET/CT imaging parameters for prediction of treatment outcome in Hodgkin and diffuse large B cell lymphoma: A systematic review. *European Journal of Nuclear Medicine and Molecular Imaging*, *48*(10), 3198–3220. https://doi.org/10.1007/s00259-021-05233-2

Green, T. M., Young, K. H., Visco, C., Xu-Monette, Z. Y., Orazi, A., Go, R. S., Nielsen, O., Gadeberg, O. V., Mourits-Andersen, T., Frederiksen, M., Pedersen, L. M., & Møller, M. B. (2012). Immunohistochemical Double-Hit Score Is a Strong Predictor of Outcome in Patients With Diffuse Large B-Cell Lymphoma Treated With Rituximab Plus Cyclophosphamide, Doxorubicin, Vincristine, and Prednisone. *Journal of Clinical Oncology*, *30*(28), 3460–3467. https://doi.org/10.1200/JCO.2011.41.4342

Grommes, C., Pastore, A., Palaskas, N., Tang, S. S., Campos, C., Schartz, D., Codega, P., Nichol, D., Clark, O., Hsieh, W.-Y., Rohle, D., Rosenblum, M., Viale, A., Tabar, V. S., Brennan, C. W., Gavrilovic, I. T., Kaley, T. J., Nolan, C. P., Omuro, A., … Mellinghoff, I. K. (2017). Ibrutinib Unmasks Critical Role of Bruton Tyrosine Kinase in Primary CNS Lymphoma. *Cancer Discovery*, *7*(9), 1018–1029. https://doi.org/10.1158/2159-8290.CD-17-0613

Heitzer, E., Haque, I. S., Roberts, C. E. S., & Speicher, M. R. (2019). Current and future perspectives of liquid biopsies in genomics-driven oncology. *Nature Reviews Genetics*, *20*(2), 71–88. https://doi.org/10.1038/s41576-018-0071-5

Iqbal, J., Greiner, T. C., Patel, K., Dave, B. J., Smith, L., Ji, J., Wright, G., Sanger, W. G., Pickering, D. L., Jain, S., Horsman, D. E., Shen, Y., Fu, K., Weisenburger, D. D., Hans, C. P., Campo, E., Gascoyne, R. D., Rosenwald, A., Jaffe, E. S., … for the Leukemia/Lymphoma Molecular Profiling Project (LLMPP). (2007). Distinctive patterns of BCL6 molecular alterations and their functional consequences in different subgroups of diffuse large B-cell lymphoma. *Leukemia*, *21*(11), 2332–2343. https://doi.org/10.1038/sj.leu.2404856

Jamal, E., Poynton, E., Elbogdady, M., Shamaa, S., & Okosun, J. (2024). Prospects for liquid biopsy approaches in lymphomas. *Leukemia & Lymphoma*, *65*(13), 1923–1933. https://doi.org/10.1080/10428194.2024.2389210

Karube, K., & Campo, E. (2015). MYC Alterations in Diffuse Large B-Cell Lymphomas. *Seminars in Hematology*, *52*(2), 97–106. https://doi.org/10.1053/j.seminhematol.2015.01.009

Karube, K., Enjuanes, A., Dlouhy, I., Jares, P., Martin-Garcia, D., Nadeu, F., Ordóñez, G. R., Rovira, J., Clot, G., Royo, C., Navarro, A., Gonzalez-Farre, B., Vaghefi, A., Castellano, G., Rubio-Perez, C., Tamborero, D., Briones, J., Salar, A., Sancho, J. M., … Campo, E. (2018). Integrating genomic alterations in diffuse large B-cell lymphoma identifies new relevant pathways and potential therapeutic targets. *Leukemia*, *32*(3), 675–684. https://doi.org/10.1038/leu.2017.251

Kato, M., Sanada, M., Kato, I., Sato, Y., Takita, J., Takeuchi, K., Niwa, A., Chen, Y., Nakazaki, K., Nomoto, J., Asakura, Y., Muto, S., Tamura, A., Iio, M., Akatsuka, Y., Hayashi, Y., Mori, H.,

Igarashi, T., Kurokawa, M., … Ogawa, S. (2009). Frequent inactivation of A20 in B-cell lymphomas. *Nature*, *459*(7247), 712–716. https://doi.org/10.1038/nature07969

Kerbauy, F. R., Colleoni, G. W., Saad, S. T., Regis Silva, M. R., Correa Alves, A., Aguiar, K. C., Albuquerque, D. M., Kobarg, J., Seixas, M. T., & Kerbauy, J. (2004). Detection and Possible Prognostic Relevance of *p53* Gene Mutations in Diffuse Large B-cell Lymphoma. An Analysis of 51 Cases and Review of the Literature. *Leukemia & Lymphoma*, *45*(10), 2071–2078. https://doi.org/10.1080/10428190410001713170

Knies, N., Alankus, B., Weilemann, A., Tzankov, A., Brunner, K., Ruff, T., Kremer, M., Keller, U. B., Lenz, G., & Ruland, J. (2015). Lymphomagenic CARD11/BCL10/MALT1 signaling drives malignant B-cell proliferation via cooperative NF-κB and JNK activation. *Proceedings of the National Academy of Sciences*, *112*(52). https://doi.org/10.1073/pnas.1507459112

Kurtz, D. M., Green, M. R., Bratman, S. V., Scherer, F., Liu, C. L., Kunder, C. A., Takahashi, K., Glover, C., Keane, C., Kihira, S., Visser, B., Callahan, J., Kong, K. A., Faham, M., Corbelli, K. S., Miklos, D., Advani, R. H., Levy, R., Hicks, R. J., … Alizadeh, A. A. (2015). Noninvasive monitoring of diffuse large B-cell lymphoma by immunoglobulin high-throughput sequencing. *Blood*, *125*(24), 3679–3687. https://doi.org/10.1182/blood-2015-03-635169

Kurtz, D. M., Scherer, F., Jin, M. C., Soo, J., Craig, A. F. M., Esfahani, M. S., Chabon, J. J., Stehr, H., Liu, C. L., Tibshirani, R., Maeda, L. S., Gupta, N. K., Khodadoust, M. S., Advani, R. H., Levy, R., Newman, A. M., Dührsen, U., Hüttmann, A., Meignan, M., … Alizadeh, A. A. (2018). Circulating Tumor DNA Measurements As Early Outcome Predictors in Diffuse Large B-Cell Lymphoma. *Journal of Clinical Oncology*, *36*(28), 2845–2853. https://doi.org/10.1200/JCO.2018.78.5246

Kwak, J.-Y. (2012). Treatment of Diffuse Large B Cell Lymphoma. *The Korean Journal of Internal Medicine*, *27*(4), 369. https://doi.org/10.3904/kjim.2012.27.4.369

Lam, L. T., Wright, G., Davis, R. E., Lenz, G., Farinha, P., Dang, L., Chan, J. W., Rosenwald, A., Gascoyne, R. D., & Staudt, L. M. (2008). Cooperative signaling through the signal transducer and activator of transcription 3 and nuclear factor-κB pathways in subtypes of diffuse large B-cell lymphoma. *Blood*, *111*(7), 3701–3713. https://doi.org/10.1182/blood-2007-09-111948

Lauer, E. M., Mutter, J., & Scherer, F. (2022). Circulating tumor DNA in B-cell lymphoma: Technical advances, clinical applications, and perspectives for translational research. *Leukemia*, *36*(9), 2151–2164. https://doi.org/10.1038/s41375-022-01618-w

Lenz, G., Davis, R. E., Ngo, V. N., Lam, L., George, T. C., Wright, G. W., Dave, S. S., Zhao, H., Xu, W., Rosenwald, A., Ott, G., Muller-Hermelink, H. K., Gascoyne, R. D., Connors, J. M., Rimsza, L. M., Campo, E., Jaffe, E. S., Delabie, J., Smeland, E. B., … Staudt, L. M. (2008). Oncogenic *CARD11* Mutations in Human Diffuse Large B Cell Lymphoma. *Science*, *319*(5870), 1676–1679. https://doi.org/10.1126/science.1153629

Lionakis, M. S., Dunleavy, K., Roschewski, M., Widemann, B. C., Butman, J. A., Schmitz, R., Yang, Y., Cole, D. E., Melani, C., Higham, C. S., Desai, J. V., Ceribelli, M., Chen, L., Thomas, C. J., Little, R. F., Gea-Banacloche, J., Bhaumik, S., Stetler-Stevenson, M., Pittaluga, S., … Wilson, W. H. (2017). Inhibition of B Cell Receptor Signaling by Ibrutinib in Primary CNS Lymphoma. *Cancer Cell*, *31*(6), 833-843.e5. https://doi.org/10.1016/j.ccell.2017.04.012

Liu, Y., & Barta, S. K. (2019). Diffuse large B-cell lymphoma: 2019 update on diagnosis, risk stratification, and treatment. *American Journal of Hematology*, *94*(5), 604–616. https://doi.org/10.1002/ajh.25460

Lugtenburg, P. J., De Nully Brown, P., Van Der Holt, B., D'Amore, F. A., Koene, H. R., De Jongh, E., Fijnheer, R., Van Esser, J. W., Böhmer, L. H., Pruijt, J. F., Verhoef, G. E., Hoogendoorn, M., Bilgin, M. Y., Nijland, M., Van Der Burg-de Graauw, N. C., Oosterveld, M., Jie, K.-S. G., Larsen, T. S., Van Der Poel, M. W., … Zijlstra-Baalbergen, J. M. (2020). Rituximab-CHOP With Early Rituximab Intensification for Diffuse Large B-Cell Lymphoma: A Randomized Phase III Trial of the HOVON and the Nordic Lymphoma Group (HOVON-84). *Journal of Clinical Oncology*, *38*(29), 3377–3387. https://doi.org/10.1200/JCO.19.03418

Mathews Griner, L. A., Guha, R., Shinn, P., Young, R. M., Keller, J. M., Liu, D., Goldlust, I. S., Yasgar, A., McKnight, C., Boxer, M. B., Duveau, D. Y., Jiang, J.-K., Michael, S., Mierzwa, T., Huang, W., Walsh, M. J., Mott, B. T., Patel, P., Leister, W., … Thomas, C. J. (2014). High-throughput combinatorial screening identifies drugs that cooperate with ibrutinib to kill activated B-cell–like diffuse large B-cell lymphoma cells. *Proceedings of the National Academy of Sciences*, *111*(6), 2349–2354. https://doi.org/10.1073/pnas.1311846111

Mendeville, M. S., Janssen, J., Los-de Vries, G. T., Van Dijk, E., Richter, J., Nijland, M., Roemer, M. G. M., Stathi, P., Hijmering, N. J., Bladergroen, R., Pelaz, D. A., Diepstra, A., Eertink, C. J., Burggraaff, C. N., Kim, Y., Lugtenburg, P. J., Van Den Berg, A., Tzankov, A., Dirnhofer, S., … De Jong, D. (2025). Integrating genetic subtypes with PET scan monitoring to predict outcome in diffuse large B-cell lymphoma. *Nature Communications*, *16*(1), 109. https://doi.org/10.1038/s41467-024-55614-y

Meriranta, L., Alkodsi, A., Pasanen, A., Lepistö, M., Mapar, P., Blaker, Y. N., Jørgensen, J., Karjalainen-Lindsberg, M.-L., Fiskvik, I., Mikalsen, L. T. G., Autio, M., Björkholm, M., Jerkeman, M., Fluge, Ø., Brown, P., Jyrkkiö, S., Holte, H., Pitkänen, E., Ellonen, P., & Leppä, S. (2022). Molecular features encoded in the ctDNA reveal heterogeneity and predict outcome in high-risk

aggressive B-cell lymphoma. *Blood*, *139*(12), 1863–1877. https://doi.org/10.1182/blood.2021012852

Mesin, L., Ersching, J., & Victora, G. D. (2016). Germinal Center B Cell Dynamics. *Immunity*, *45*(3), 471–482. https://doi.org/10.1016/j.immuni.2016.09.001

Mikhaeel, N. G., Heymans, M. W., Eertink, J. J., De Vet, H. C. W., Boellaard, R., Dührsen, U., Ceriani, L., Schmitz, C., Wiegers, S. E., Hüttmann, A., Lugtenburg, P. J., Zucca, E., Zwezerijnen, G. J. C., Hoekstra, O. S., Zijlstra, J. M., & Barrington, S. F. (2022). Proposed New Dynamic Prognostic Index for Diffuse Large B-Cell Lymphoma: International Metabolic Prognostic Index. *Journal of Clinical Oncology*, *40*(21), 2352–2360. https://doi.org/10.1200/JCO.21.02063

Moia, R., Favini, C., Ferri, V., Forestieri, G., Terzi Di Bergamo, L., Schipani, M., Sagiraju, S., Andorno, A., Rasi, S., Adhinaveni, R., Talotta, D., Al Essa, W., De Paoli, L., Margiotta Casaluci, G., Patriarca, A., Boldorini, R. L., Rossi, D., & Gaidano, G. (2021). Multiregional sequencing and circulating tumour DNA analysis provide complementary approaches for comprehensive disease profiling of small lymphocytic lymphoma. *British Journal of Haematology*, *195*(1), 108–112. https://doi.org/10.1111/bjh.17718

Moia, R., Talotta, D., Terzi Di Bergamo, L., Almasri, M., Dondolin, R., Salehi, M., Cosentino, C., Soscia, R., Della Starza, I., Bruscaggin, A., Andorno, A., Mercalli, F., Cresta, S., Bomben, R., Bittolo, T., Vit, F., Bulian, P., Zucchetto, A., Bruna, R., … Gaidano, G. (2025). Molecular clustering on ctDNA improves the prognostic stratification of patients with DLBCL compared with ctDNA levels. *Blood Advances*, *9*(7), 1692–1701. https://doi.org/10.1182/bloodadvances.2024014136

Morin, R. D., Mendez-Lago, M., Mungall, A. J., Goya, R., Mungall, K. L., Corbett, R. D., Johnson, N. A., Severson, T. M., Chiu, R., Field, M., Jackman, S., Krzywinski, M., Scott, D. W., Trinh, D. L., Tamura-Wells, J., Li, S., Firme, M. R., Rogic, S., Griffith, M., … Marra, M. A. (2011). Frequent mutation of histone-modifying genes in non-Hodgkin lymphoma. *Nature*, *476*(7360), 298–303. https://doi.org/10.1038/nature10351

Muppidi, J. R., Schmitz, R., Green, J. A., Xiao, W., Larsen, A. B., Braun, S. E., An, J., Xu, Y., Rosenwald, A., Ott, G., Gascoyne, R. D., Rimsza, L. M., Campo, E., Jaffe, E. S., Delabie, J., Smeland, E. B., Braziel, R. M., Tubbs, R. R., Cook, J. R., … Cyster, J. G. (2014). Loss of signalling via Gα13 in germinal centre B-cell-derived lymphoma. *Nature*, *516*(7530), 254–258. https://doi.org/10.1038/nature13765

Ngo, V. N., Young, R. M., Schmitz, R., Jhavar, S., Xiao, W., Lim, K.-H., Kohlhammer, H., Xu, W., Yang, Y., Zhao, H., Shaffer, A. L., Romesser, P., Wright, G., Powell, J., Rosenwald, A., Muller-Hermelink, H. K., Ott, G., Gascoyne, R. D., Connors, J. M., … Staudt, L. M. (2011). Oncogenically active MYD88 mutations in human lymphoma. *Nature*, *470*(7332), 115–119. https://doi.org/10.1038/nature09671

Pasqualucci, L., Compagno, M., Houldsworth, J., Monti, S., Grunn, A., Nandula, S. V., Aster, J. C., Murty, V. V., Shipp, M. A., & Dalla-Favera, R. (2006). Inactivation of the PRDM1/BLIMP1 gene in diffuse large B cell lymphoma. *The Journal of Experimental Medicine*, *203*(2), 311–317. https://doi.org/10.1084/jem.20052204

Pasqualucci, L., & Dalla-Favera, R. (2018a). Genetics of diffuse large B-cell lymphoma. *Blood*, *131*(21), 2307–2319. https://doi.org/10.1182/blood-2017-11-764332

Pasqualucci, L., & Dalla-Favera, R. (2018b). Genetics of diffuse large B-cell lymphoma. *Blood*, *131*(21), 2307–2319. https://doi.org/10.1182/blood-2017-11-764332

Pasqualucci, L., Trifonov, V., Fabbri, G., Ma, J., Rossi, D., Chiarenza, A., Wells, V. A., Grunn, A., Messina, M., Elliot, O., Chan, J., Bhagat, G., Chadburn, A., Gaidano, G., Mullighan, C. G., Rabadan, R., & Dalla-Favera, R. (2011). Analysis of the coding genome of diffuse large B-cell lymphoma. *Nature Genetics*, *43*(9), 830–837. https://doi.org/10.1038/ng.892

Phillips, T. J., Forero-Torres, A., Sher, T., Diefenbach, C. S., Johnston, P., Talpaz, M., Pulini, J., Zhou, L., Scherle, P., Chen, X., & Barr, P. M. (2018). Phase 1 study of the PI3Kδ inhibitor INCB040093 ± JAK1 inhibitor itacitinib in relapsed/refractory B-cell lymphoma. *Blood*, *132*(3), 293–306. https://doi.org/10.1182/blood-2017-10-812701

Quintanilla-Martinez, L. (2017). The 2016 updated WHO classification of lymphoid neoplasias. *Hematological Oncology*, *35*(S1), 37–45. https://doi.org/10.1002/hon.2399

Rhyasen, G. W., & Starczynowski, D. T. (2015). IRAK signalling in cancer. *British Journal of Cancer*, *112*(2), 232–237. https://doi.org/10.1038/bjc.2014.513

Rivas-Delgado, A., Nadeu, F., Enjuanes, A., Casanueva-Eliceiry, S., Mozas, P., Magnano, L., Castrejón De Anta, N., Rovira, J., Dlouhy, I., Martín, S., Osuna, M., Rodríguez, S., Simó, M., Pinyol, M., Baumann, T., Beà, S., Balagué, O., Delgado, J., Villamor, N., … López-Guillermo, A. (2021). Mutational Landscape and Tumor Burden Assessed by Cell-free DNA in Diffuse Large B-Cell Lymphoma in a Population-Based Study. *Clinical Cancer Research*, *27*(2), 513–521. https://doi.org/10.1158/1078-0432.CCR-20-2558

Roschewski, M., Lindenberg, L., Mena, E., Lakhotia, R., Melani, C., Steinberg, S. M., Schultz, A., Hogan, G., Chabon, J. J., Close, S., Diehn, M., Sworder, B. J., Kurtz, D. M., Alizadeh, A. A., &

Wilson, W. H. (2023). End-of-Treatment Response Assessment after Frontline Therapy for Aggressive B-Cell Lymphoma: Landmark Comparison of a Singular PET/CT Scan Versus Ultrasensitive Circulating Tumor DNA. *Blood*, *142*(Supplement 1), 192–192. https://doi.org/10.1182/blood-2023-180007

Roschewski, M., Staudt, L. M., & Wilson, W. H. (2014). Diffuse large B-cell lymphoma—Treatment approaches in the molecular era. *Nature Reviews Clinical Oncology*, *11*(1), 12–23. https://doi.org/10.1038/nrclinonc.2013.197

Rosenthal, A., & Younes, A. (2017). High grade B-cell lymphoma with rearrangements of MYC and BCL2 and/or BCL6: Double hit and triple hit lymphomas and double expressing lymphoma. *Blood Reviews*, *31*(2), 37–42. https://doi.org/10.1016/j.blre.2016.09.004

Rosenwald, A., Wright, G., Chan, W. C., Connors, J. M., Campo, E., Fisher, R. I., Gascoyne, R. D., Muller-Hermelink, H. K., Smeland, E. B., Giltnane, J. M., Hurt, E. M., Zhao, H., Averett, L., Yang, L., Wilson, W. H., Jaffe, E. S., Simon, R., Klausner, R. D., Powell, J., … Staudt, L. M. (2002). The Use of Molecular Profiling to Predict Survival after Chemotherapy for Diffuse Large-B-Cell Lymphoma. *New England Journal of Medicine*, *346*(25), 1937–1947. https://doi.org/10.1056/NEJMoa012914

Rossi, D., Diop, F., Spaccarotella, E., Monti, S., Zanni, M., Rasi, S., Deambrogi, C., Spina, V., Bruscaggin, A., Favini, C., Serra, R., Ramponi, A., Boldorini, R., Foà, R., & Gaidano, G. (2017). Diffuse large B-cell lymphoma genotyping on the liquid biopsy. *Blood*, *129*(14), 1947–1957. https://doi.org/10.1182/blood-2016-05-719641

Sasanelli, M., Meignan, M., Haioun, C., Berriolo-Riedinger, A., Casasnovas, R.-O., Biggi, A., Gallamini, A., Siegel, B. A., Cashen, A. F., Véra, P., Tilly, H., Versari, A., & Itti, E. (2014).

Pretherapy metabolic tumour volume is an independent predictor of outcome in patients with diffuse large B-cell lymphoma. *European Journal of Nuclear Medicine and Molecular Imaging*, *41*(11), 2017–2022. https://doi.org/10.1007/s00259-014-2822-7

Savino, F. D., Rigali, F., Giustini, V., D'Aliberti, D., Spinelli, S., Piazza, R., Sacco, A., & Roccaro, A. M. (2022). Liquid Biopsy in Cancer: Focus on Lymphoproliferative Disorders. *Cancers*, *14*(21), 5378. https://doi.org/10.3390/cancers14215378

Scherer, F., Kurtz, D. M., Newman, A. M., Stehr, H., Craig, A. F. M., Esfahani, M. S., Lovejoy, A. F., Chabon, J. J., Klass, D. M., Liu, C. L., Zhou, L., Glover, C., Visser, B. C., Poultsides, G. A., Advani, R. H., Maeda, L. S., Gupta, N. K., Levy, R., Ohgami, R. S., … Alizadeh, A. A. (2016). Distinct biological subtypes and patterns of genome evolution in lymphoma revealed by circulating tumor DNA. *Science Translational Medicine*, *8*(364). https://doi.org/10.1126/scitranslmed.aai8545

Schmitz, R., Wright, G. W., Huang, D. W., Johnson, C. A., Phelan, J. D., Wang, J. Q., Roulland, S., Kasbekar, M., Young, R. M., Shaffer, A. L., Hodson, D. J., Xiao, W., Yu, X., Yang, Y., Zhao, H., Xu, W., Liu, X., Zhou, B., Du, W., … Staudt, L. M. (2018). Genetics and Pathogenesis of Diffuse Large B-Cell Lymphoma. *New England Journal of Medicine*, *378*(15), 1396–1407. https://doi.org/10.1056/NEJMoa1801445

Scott, D. W., Mottok, A., Ennishi, D., Wright, G. W., Farinha, P., Ben-Neriah, S., Kridel, R., Barry, G. S., Hother, C., Abrisqueta, P., Boyle, M., Meissner, B., Telenius, A., Savage, K. J., Sehn, L. H., Slack, G. W., Steidl, C., Staudt, L. M., Connors, J. M., … Gascoyne, R. D. (2015). Prognostic Significance of Diffuse Large B-Cell Lymphoma Cell of Origin Determined by Digital Gene Expression in Formalin-Fixed Paraffin-Embedded Tissue Biopsies. *Journal of Clinical Oncology*, *33*(26), 2848–2856. https://doi.org/10.1200/JCO.2014.60.2383

Sehn, L. H., & Salles, G. (2021). Diffuse Large B-Cell Lymphoma. *New England Journal of Medicine*, *384*(9), 842–858. https://doi.org/10.1056/NEJMra2027612

Shilatifard, A. (2012). The COMPASS Family of Histone H3K4 Methylases: Mechanisms of Regulation in Development and Disease Pathogenesis. *Annual Review of Biochemistry*, *81*(1), 65–95. https://doi.org/10.1146/annurev-biochem-051710-134100

Sneeringer, C. J., Scott, M. P., Kuntz, K. W., Knutson, S. K., Pollock, R. M., Richon, V. M., & Copeland, R. A. (2010). Coordinated activities of wild-type plus mutant EZH2 drive tumor-associated hypertrimethylation of lysine 27 on histone H3 (H3K27) in human B-cell lymphomas. *Proceedings of the National Academy of Sciences*, *107*(49), 20980–20985. https://doi.org/10.1073/pnas.1012525107

Soscia, R., Assanto, G. M., Starza, I. D., Moia, R., Talotta, D., Bellomarino, V., Bellissimo, T., Antonacci, M., Petrucci, L., Gaidano, G., Guarini, A., Martelli, M., Di Rocco, A., Foà, R., & Del Giudice, I. (2024). Molecular measurable residual disease by immunoglobulin gene rearrangements on circulating tumor DNA predicts outcome in diffuse large B-cell lymphoma. *Haematologica*. https://doi.org/10.3324/haematol.2024.286331

Spina, V., Bruscaggin, A., Cuccaro, A., Martini, M., Di Trani, M., Forestieri, G., Manzoni, M., Condoluci, A., Arribas, A., Terzi-Di-Bergamo, L., Locatelli, S. L., Cupelli, E., Ceriani, L., Moccia, A. A., Stathis, A., Nassi, L., Deambrogi, C., Diop, F., Guidetti, F., … Rossi, D. (2018). Circulating tumor DNA reveals genetics, clonal evolution, and residual disease in classical Hodgkin lymphoma. *Blood*, *131*(22), 2413–2425. https://doi.org/10.1182/blood-2017-11-812073

Stebegg, M., Kumar, S. D., Silva-Cayetano, A., Fonseca, V. R., Linterman, M. A., & Graca, L. (2018). Regulation of the Germinal Center Response. *Frontiers in Immunology*, *9*, 2469. https://doi.org/10.3389/fimmu.2018.02469

Steinberg, M. W., Cheung, T. C., & Ware, C. F. (2011). The signaling networks of the herpesvirus entry mediator (TNFRSF14) in immune regulation. *Immunological Reviews*, *244*(1), 169–187. https://doi.org/10.1111/j.1600-065X.2011.01064.x

Talotta, D., Almasri, M., Cosentino, C., Gaidano, G., & Moia, R. (2023). Liquid biopsy in hematological malignancies: Current and future applications. *Frontiers in Oncology*, *13*, 1164517. https://doi.org/10.3389/fonc.2023.1164517

Thieblemont, C., Briere, J., Mounier, N., Voelker, H.-U., Cuccuini, W., Hirchaud, E., Rosenwald, A., Jack, A., Sundstrom, C., Cogliatti, S., Trougouboff, P., Boudova, L., Ysebaert, L., Soulier, J., Chevalier, C., Bron, D., Schmitz, N., Gaulard, P., Houlgatte, R., & Gisselbrecht, C. (2011). The Germinal Center/Activated B-Cell Subclassification Has a Prognostic Impact for Response to Salvage Therapy in Relapsed/Refractory Diffuse Large B-Cell Lymphoma: A Bio-CORAL Study. *Journal of Clinical Oncology*, *29*(31), 4079–4087. https://doi.org/10.1200/JCO.2011.35.4423

Thome, M. (2004). CARMA1, BCL-10 and MALT1 in lymphocyte development and activation. *Nature Reviews Immunology*, *4*(5), 348–359. https://doi.org/10.1038/nri1352

Tilly, H., Gomes Da Silva, M., Vitolo, U., Jack, A., Meignan, M., Lopez-Guillermo, A., Walewski, J., André, M., Johnson, P. W., Pfreundschuh, M., & Ladetto, M. (2015). Diffuse large B-cell lymphoma (DLBCL): ESMO Clinical Practice Guidelines for diagnosis, treatment and follow-up. *Annals of Oncology*, *26*, v116–v125. https://doi.org/10.1093/annonc/mdv304

Tilly, H., Morschhauser, F., Sehn, L. H., Friedberg, J. W., Trněný, M., Sharman, J. P., Herbaux, C., Burke, J. M., Matasar, M., Rai, S., Izutsu, K., Mehta-Shah, N., Oberic, L., Chauchet, A., Jurczak, W., Song, Y., Greil, R., Mykhalska, L., Bergua-Burgués, J. M., … Salles, G. (2022). Polatuzumab Vedotin in Previously Untreated Diffuse Large B-Cell Lymphoma. *New England Journal of Medicine*, *386*(4), 351–363. https://doi.org/10.1056/NEJMoa2115304

Trinh, D. L., Scott, D. W., Morin, R. D., Mendez-Lago, M., An, J., Jones, S. J. M., Mungall, A. J., Zhao, Y., Schein, J., Steidl, C., Connors, J. M., Gascoyne, R. D., & Marra, M. A. (2013). Analysis of FOXO1 mutations in diffuse large B-cell lymphoma. *Blood*, *121*(18), 3666–3674. https://doi.org/10.1182/blood-2013-01-479865

Vercellino, L., Cottereau, A.-S., Casasnovas, O., Tilly, H., Feugier, P., Chartier, L., Fruchart, C., Roulin, L., Oberic, L., Pica, G. M., Ribrag, V., Abraham, J., Simon, M., Gonzalez, H., Bouabdallah, R., Fitoussi, O., Sebban, C., López-Guillermo, A., Sanhes, L., … Thieblemont, C. (2020). High total metabolic tumor volume at baseline predicts survival independent of response to therapy. *Blood*, *135*(16), 1396–1405. https://doi.org/10.1182/blood.2019003526

Wilson, W. H., Young, R. M., Schmitz, R., Yang, Y., Pittaluga, S., Wright, G., Lih, C.-J., Williams, P. M., Shaffer, A. L., Gerecitano, J., De Vos, S., Goy, A., Kenkre, V. P., Barr, P. M., Blum, K. A., Shustov, A., Advani, R., Fowler, N. H., Vose, J. M., … Staudt, L. M. (2015). Targeting B cell receptor signaling with ibrutinib in diffuse large B cell lymphoma. *Nature Medicine*, *21*(8), 922–926. https://doi.org/10.1038/nm.3884

Wright, G. W., Huang, D. W., Phelan, J. D., Coulibaly, Z. A., Roulland, S., Young, R. M., Wang, J. Q., Schmitz, R., Morin, R. D., Tang, J., Jiang, A., Bagaev, A., Plotnikova, O., Kotlov, N., Johnson, C. A., Wilson, W. H., Scott, D. W., & Staudt, L. M. (2020). A Probabilistic Classification

Tool for Genetic Subtypes of Diffuse Large B Cell Lymphoma with Therapeutic Implications. *Cancer Cell*, *37*(4), 551-568.e14. https://doi.org/10.1016/j.ccell.2020.03.015

Xu-Monette, Z. Y., Wu, L., Visco, C., Tai, Y. C., Tzankov, A., Liu, W., Montes-Moreno, S., Dybkær, K., Chiu, A., Orazi, A., Zu, Y., Bhagat, G., Richards, K. L., Hsi, E. D., Zhao, X. F., Choi, W. W. L., Zhao, X., Van Krieken, J. H., Huang, Q., … Young, K. H. (2012). Mutational profile and prognostic significance of TP53 in diffuse large B-cell lymphoma patients treated with R-CHOP: Report from an International DLBCL Rituximab-CHOP Consortium Program Study. *Blood*, *120*(19), 3986–3996. https://doi.org/10.1182/blood-2012-05-433334

Young, K. H., Weisenburger, D. D., Dave, B. J., Smith, L., Sanger, W., Iqbal, J., Campo, E., Delabie, J., Gascoyne, R. D., Ott, G., Rimsza, L., Müller-Hermelink, H. K., Jaffe, E. S., Rosenwald, A., Staudt, L. M., Chan, W. C., & Greiner, T. C. (2007). Mutations in the DNA-binding codons of TP53, which are associated with decreased expression of TRAILreceptor-2, predict for poor survival in diffuse large B-cell lymphoma. *Blood*, *110*(13), 4396–4405. https://doi.org/10.1182/blood-2007-02-072082

Zhang, Y., Song, L., Zhao, M., & Hu, K. (2019). A better prediction of progression-free survival in diffuse large B-cell lymphoma by a prognostic model consisting of baseline TLG and $\%\Delta SUV_{max}$. *Cancer Medicine*, *8*(11), 5137–5147. https://doi.org/10.1002/cam4.2284

Zwanenburg, A., Vallières, M., Abdalah, M. A., Aerts, H. J. W. L., Andrearczyk, V., Apte, A., Ashrafinia, S., Bakas, S., Beukinga, R. J., Boellaard, R., Bogowicz, M., Boldrini, L., Buvat, I., Cook, G. J. R., Davatzikos, C., Depeursinge, A., Desseroit, M.-C., Dinapoli, N., Dinh, C. V., … Löck, S. (2020). The Image Biomarker Standardization Initiative: Standardized Quantitative Radiomics for High-Throughput Image-based Phenotyping. *Radiology*, *295*(2), 328–338. https://doi.org/10.1148/radiol.2020191145

ACKNOWLEDGEMENT

I am profoundly grateful to **Professor Gianluca Gaidano** for the expert mentorship and vision provided over the course of this thesis. Their commitment to excellence and academic integrity has been a constant inspiration. This work would not have been possible without his technical expertise and encouragement."

Special thanks go to **Colleague's in my lab** for the collaborative spirit and technical assistance provided in the lab. Their contributions to our discussions and their willingness to lend a hand during data collection were instrumental to the success of this research."

To my family, thank you for being my rock. Your unwavering belief in me, even when I doubted myself, provided the strength I needed to cross the finish line. Thank you for your endless patience, your love, and for always reminding me that there is a world outside the laboratory. This achievement is as much yours as it is mine."